1 **Title: Flask measurements of long-lived trace gases at three ground stations in India**

2

3 X. Lin[1], N. K. Indira[2], M. Ramonet[1], M. Delmotte[1], P. Ciais[1], B. C. Bhatt[3], M. V. Reddy[4], D.

4 Angchuk[3], S. Balakrishnan[4], S. Jorphail[3], T. Dorjai[3], T. T. Mahey[3], S. Patnaik[4], M. Begum[5],

5 C. Brenninkmeijer[6], S. Durairaj[5], R. Kirubagaran[7], M. Schmidt[1,8], P. S. Swathi[2], N. V.

6 Vinithkumar[5], C. Yver Kwok[1], and V. K. Gaur[2]

7

8 [1] Laboratoire des Sciences du Climat et de l'Environnement (LSCE), UMR CEA-CNRS-
9 UVSQ, Gif-sur-Yvette 91191, France

10 [2] CSIR Fourth Paradigm Institute (formerly CSIR Centre for Mathematical Modelling and
11 Computer Simulation), NAL Belur Campus, Bangalore 560 037, India

12 [3] Indian Institute of Astrophysics, Bangalore 560 034, India

13 [4] Department of Earth Sciences, Pondicherry University, Puducherry 605 014, India

14 [5] Andaman and Nicobar Centre for Ocean Science and Technology (ANCOST), ESSO-NIOT,
15 Port Blair 744103, Andaman and Nicobar Islands, India

16 [6] Max Planck Institute for Chemistry, Hahn-Meitner-Weg 1, D-55128 Mainz, Germany

17 [7] Earth System Sciences Organisation - National Institute of Ocean Technology (ESSO-
18 NIOT), Ministry of Earth Sciences, Government of India, Tamil Nadu, Chennai 600 100,
19 India

20 [8] Institut für Umweltphysik, Universität Heidelberg, INF 229, 69120 Heidelberg, Germany

21

22   **Abstract**

23   With a rapid growth in population and economic development, emissions of greenhouse

24   gases (GHGs) from the Indian subcontinent have sharply increased during recent decades.

25   However, evaluation of regional fluxes of GHGs and characterization of their spatial and

26   temporal variations by atmospheric inversions remain uncertain due to a sparse regional

27   atmospheric observation network. As a result of an Indo-French collaboration, three new

28   atmospheric stations were established in India at Hanle (HLE), Pondicherry (PON) and Port

29   Blair (PBL), with the objective of monitoring the atmospheric concentrations of GHGs and

30   other trace gases. Here we present the results of the measurements of CO_2, CH_4, N_2O, SF_6,

31   CO, and H_2 from regular flask sampling at these three stations over the period 2007–2011.

32   For each species, annual means, seasonal cycles and gradients between stations were

33   calculated and related to variations in the natural GHG fluxes, anthropogenic emissions, and

34   the monsoon circulations. Covariances between species at the synoptic scale were analyzed to

35   investigate the likely source(s) of emissions. The flask measurements of various trace gases at

36   the three stations show potential to constrain the inversions of fluxes over Southern and

37   Northeastern India. However, this network of ground stations needs further extension to other

38   parts of India to better constrain the GHG budgets at regional and continental scales.

39

1 Introduction

Since the pre-industrial times, anthropogenic greenhouse gas (GHG) emissions have progressively increased the radiative forcing of the atmosphere, leading to impacts on the climate system and human society (IPCC, 2013, 2014a, b). With rapid socio-economic development and urbanization during recent decades, a large and growing share of GHG emissions is contributed by emerging economies like China and India. In 2010, India became the world's third largest GHG emitter, next to China and the USA (EDGAR v4.2; Le Quéré et al., 2014). Between 1991 and 2010, anthropogenic GHG emissions in India increased by ~100% from 1.4 to 2.8 $GtCO_2eq$, much faster than rates of most developed countries and economies like the USA (9%) and EU (-14%) over the same period (EDGAR v4.2). Without a systematic effort at mitigation, this trend would continue in the coming decades, given that the per capita emission rate in India is still much below that of the more developed countries. For comparison, in 2010, the per capita GHG emission rates were 2.2, 10.9, 17.6, and 21.6 $tonCO_2eq$/capita for India, the UK, Russia, and the USA, respectively (EDGAR v4.2). In particular, non-CO_2 GHG emissions are substantial in India, most of which are contributed by agricultural activities over populous rural areas (Pathak et al., 2010). In 2010, anthropogenic CH_4 and N_2O emissions in India amounted to 29.6 $TgCH_4$ ($\approx$0.62 $GtCO_2eq$) and 0.8 TgN_2O ($\approx$0.23 $GtCO_2eq$), together accounting for 32% of the country's GHG emissions, of which contributions of the agricultural sector were 60 and 73%, respectively (EDGAR v4.2). Reducing emissions of these two non-CO_2 GHGs may offer a more cost-effective way to mitigate future climate change than by attempting to directly reduce CO_2 emissions (Montzka et al., 2011).

Effective climate mitigation strategies need accurate reporting of sources and sinks of GHGs. This is also a requirement of the United Nations Framework Convention on Climate Change

(UNFCCC). Current estimates of GHG budgets in India, either from the top-down approaches (based on atmospheric inversions) or bottom-up approaches (based on emission inventories or biospheric models), have larger uncertainties than for other continents. For instance, Patra et al. (2013) reported a net biospheric CO_2 sink of -104±150 TgCyr^{-1} over South Asia during 2007–2008 based on global inversions from 10 TransCom-CO_2 models (Peylin et al., 2013) and a regional inversion (Patra et al., 2011b), while the bottom-up approach gave an estimate of -191±193 TgCyr^{-1} over the period of 2000–2009 (Patra et al., 2013). Notably, these estimates have uncertainties as high as 100–150%, much larger compared to those of Europe (~30%, see Luyssaert et al., 2012) and North America (~60%, see King et al., 2015), where observational networks are denser and emission inventories are more accurate. Evaluation of N_2O emissions from 5 TransCom-N_2O inversions also exhibited the largest differences over South Asia (Thompson et al., 2014b). A main source of uncertainty is the lack of atmospheric observation datasets with sufficient temporal and spatial coverage (Patra et al., 2013; Thompson et al., 2014b). Networks of atmospheric stations that were used to constrain estimates of global GHG fluxes show gaps over South Asia (Patra et al., 2011a; Thompson et al., 2014b, c; Peylin et al., 2013), with Cape Rama (CRI – 15.08°N, 73.83°E, 60m a.s.l.) on the southwest coast of India being the only Indian station (Rayner et al., 2008; Patra et al., 2009; Tiwari et al., 2011; Bhattacharya et al., 2009; Saikawa et al., 2014). Recently a few other ground stations have been established in Western India and the Himalayas to monitor GHGs and atmospheric pollutants, which are located in Sinhagad (SNG – 18.35°N, 73.75°E, 1600m a.s.l.; Tiwari and Kumar, 2012; Tiwari et al., 2014), Mount Abu (24.60°N, 72.70°E, 1700m a.s.l.; S. Lal, personal communication), Ahmedabad (23.00°N, 72.50°E, 55m a.s.l.; Lal et al., 2015), Nainital (29.37°N, 79.45°E, 1958m a.s.l.; Kumar et al., 2010) and Darjeeling (27.03°N, 88.15°E, 2194m a.s.l.; Ganesan et al., 2013). Most of these stations started to measure atmospheric GHG concentrations very

90 recently (e.g. Sinhagad – since 2009; Ahmedabad – since 2013; Mount Abu – since 2013;

91 Nainital – since 2006; Darjeeling – since 2011), and datasets are not always available. In

92 addition, aircraft and satellite observations have also been carried out and provided useful

93 constraints on estimates of GHG fluxes in this region (Park et al., 2007; Xiong et al., 2009;

94 Schuck et al., 2010; Patra et al., 2011b; Niwa et al., 2012; Zhang et al., 2014). Although

95 inclusion of measurements from South Asia significantly reduces uncertainties in top-down

96 estimates of regional GHG emissions (e.g., Huang et al., 2008; Niwa et al., 2012; Zhang et al.,

97 2014), a denser atmospheric observational network with sustained measurements is still

98 needed over this vast and fast-growing region for an improved, more detailed, and necessary

99 understanding of GHG budgets.

100

101 Besides the lack of a comprehensive observational network, the seasonally reversing Indian

102 monsoon circulations and orographic effects complicate simulation of regional atmospheric

103 transport, which contributes to uncertainty of the inverted GHG fluxes (e.g., Thompson et al.,

104 2014b). The Indian monsoon system is a prominent meteorological phenomenon in South

105 Asia, which, at lower altitudes, is characterized by strong southwesterlies from the Arabian

106 Sea to the Indian subcontinent during the boreal summer, and northeasterlies during the

107 boreal winter (Goswami, 2005). The summer monsoon is associated with deep convection,

108 which mixes the boundary layer air into the upper troposphere and lower stratosphere

109 (Schuck et al., 2010; Lawrence and Lelieveld, 2010). On the contrary, little deep convection

110 occurs over South Asia during the winter monsoon period, which carries less moisture

111 (Lawrence and Lelieveld, 2010). The Indian monsoon also impacts biogenic activities (e.g.,

112 vegetation growth, microbial activity) and GHG fluxes through its effects on rainfall

113 variations (Tiwari et al., 2013; Valsala et al., 2013; Gadgil, 2003). Given that accurate

114 atmospheric transport is critical for retrieving reliable inversion of GHG fluxes, an

115   observational network that comprises a range of altitudes including monitoring stations in

116   mountainous regions would be valuable for validating and improving atmospheric transport

117   models.

118

119   Since the 2000s, three new atmospheric ground stations have been established in India as part

120   of the Indo-French collaboration, with the objective of monitoring the atmospheric

121   concentrations of major GHGs and other trace gases in flask air samples. Of the three Indian

122   stations, Hanle (HLE) is a high-altitude station situated in the western Indian Himalayas,

123   while Pondicherry (PON) and Port Blair (PBL) are tropical surface stations located

124   respectively on the southeastern coast of South India and on an oceanic island in the

125   southeastern Bay of Bengal. In this study, we briefly describe the main features of these

126   stations and present time series of flask air sample measurements of multiple trace gases at

127   HLE, PON, and PBL over the period 2007–2011. Descriptions of the three stations as well as

128   methods used to analyze and calibrate the flask measurements are given in Sect. 2. For each

129   station, we measure the atmospheric concentrations of four major GHG species (CO_2, CH_4,

130   N_2O and SF_6) and two additional trace gases (CO and H_2). Among these trace gases, CO_2,

131   CH_4 and N_2O are the three most abundant GHGs in the atmosphere, and the UNFCCC

132   requires each Non-Annex I Party to regularly report anthropogenic emissions of these gases

133   (MoEF, 2012). Sulfur hexafluoride (SF_6) is widely considered as a good tracer for

134   anthropogenic activities with a long atmospheric lifetime and almost purely anthropogenic

135   sources (Maiss et al., 1996), and the Non-Annex I Parties are also encouraged to provide

136   information on its anthropogenic emissions (MoEF, 2012). Although CO and H_2 are not

137   GHGs by themselves, both of them play critical roles in the CH_4 budgets through reaction

138   with the free OH radicals (Ehhalt and Rohrer, 2009). Besides, CO and H_2 are good tracers for

139   biomass/biofuel burning (Andreae and Merlet, 2001), an important source of GHG emissions

140 that is quite extensive in India (Streets et al., 2003; Yevich and Logan, 2003). Time series of

141 atmospheric concentrations of all these trace gases are analyzed for each station to

142 characterize the annual means and seasonal cycles, with results and discussions presented in

143 Sect. 3. Gradients between different stations are interpreted in the context of regional flux

144 patterns and monsoon circulations (Sect. 3.1). We examine synoptic variations of CO_2, CH_4

145 and CO by analyzing the co-variances between species, using deviations from their smoothed

146 fitting curves (Sect. 3.2). Finally, we investigate two abnormal CH_4 and CO events at PBL

147 and propose likely sources and origins (Sect. 3.3). A summary of the paper as well as

148 conclusions drawn from these results are given in Sect. 4.

149

150 **2 Sampling stations and methods**

151 **2.1 Sampling stations**

152 Figure 1 and S1 in the supplement show the locations of HLE, PON, and PBL. We also

153 present five-day back-trajectories from each station for all sampling dates in April–June

154 (AMJ; Fig. 1a), July–September (JAS; Fig. 1b), October–December (OND; Fig. 1c) and

155 January–March (JFM; Fig. 1d), respectively. Note that this four-period classification scheme

156 is slightly different from the climatological seasons defined by the India Meteorological

157 Department (IMD; Attri and Tyagi, 2010), in which months of a year are categorized into the

158 pre-monsoon season (March–May), SW monsoon season (June–September), post-monsoon

159 season (October–December) and the winter season (January and February). We adapted the

160 IMD classification to facilitate better display and further analyses (e.g., Sect. 3.2), making

161 sure that samples are fairly evenly distributed across all seasons. The back-trajectories were

162 generated using the Hybrid Single Particle Lagrangian Integrated Trajectory (HYSPLIT4)

163 model (Draxler and Rolph, 2003), driven by wind fields from the Global Data Assimilation

System (GDAS) archive data based on National Centers for Environmental Prediction (NCEP) model output (https://ready.arl.noaa.gov/gdas1.php).

The Hanle (HLE) station (32.780 °N, 78.960 °E, 4517 m a.s.l.) is located in the campus of the Indian Astronomical Observatory (IAO) atop Mt. Saraswati, about 300 m above the Nilamkhul Plain in the Hanle Valley of southeastern Ladakh in northwestern Himalayas. The station was established in 2001 as a collaborative project between the Indian Institute of Astrophysics and LSCE, France. The flask sampling inlet is installed on the top of a 3 m mast fixed on the roof of a 2m high building, and the ambient air is pumped through a Dekabon tubing with a diameter of 1/4". The area around the station is a cold mountain desert, with sparse vegetation and a small population of ~1700 distributed over an area of ~20 km^2. Anthropogenic activities are limited to small-scale crop production (e.g., barley and wheat) and livestock farming (e.g., yaks, cows, goats, and sheep). The nearest populated city of Leh (34.25 °N, 78.00 °E, 3480 m a.s.l.) with ~27 000 inhabitants, lies 270 km to the northwest of this station. By virtue of its remoteness, high altitude, and negligible biotic and anthropogenic influences, HLE is representative of the background free tropospheric air masses in the northern mid-latitudes. Regular flask air sampling at this station has been operational since February, 2004, and continuous in-situ CO_2 measurements started in September, 2005. Over the period 2007–2011, a total of 188 flask sample pairs were collected at HLE. Back-trajectories show that, HLE dominantly samples air masses that pass over northern Africa and the Middle East throughout the year, and those coming from South and Southeast Asia during the SW monsoon season (Fig. 1a). More detailed station information of HLE would be found in several earlier publications (Babu et al., 2011; Moorthy et al., 2011).

The Pondicherry (PON) station (12.010 °N, 79.860 °E, 20 m a.s.l) is located on the southeast coast of India, about 8 km north of the city of Pondicherry with a population of ~240,000 (Census India, 2011). The station was established in collaboration with Pondicherry University in 2006. The flask sampling inlet, initially located on a 10 m mast fixed on the roof of the University Guest House, was later moved to a 30 m high tower in June, 2011. The ambient air is pumped from the top of the tower through a Dekabon tubing with a diameter of 1/4". The surrounding village Kalapet, has a population of ~9000 (Sivakumar and Anitha, 2012). A four-lane highway runs nearly 80 m to the west of the station with a low traffic flow especially during the nighttime, while the Indian Ocean stands about 100 m to the east of the station. Moreover, the two nearest megalopolises of Chennai and Bangalore, both with populations of over 6 million (Census India, 2011), are approximately 143 km to the north and 330 km to the west of the station. Given its proximity to an urban area and a highway, PON can be influenced by local emissions. Although the highway nearby has a low traffic flow, in-situ measurements at PON (not presented in this paper) do show that this site is heavily polluted by local emissions during nighttime. In order to minimize the influences of local GHG sources/sinks, flask air sampling at PON is performed between 12:00 and 18:00 local time (LT) (actually 97% of flask samples taken between 12:00 and 14:00 LT), when the sea breeze moves clean air masses towards the land and the boundary layer air is well mixed. Further, we also remove outliers that are likely polluted by local emissions and not representative of regional background concentrations (see Sect. 2.3.1 for details). We believe that through these two approaches the local influences at PON should be sufficiently minimized. Flask sampling at PON began in September, 2006 and over the period 2007–2011, a total of 185 flask sample pairs were collected at the site. As shown in Fig. 1a, the air masses received at PON are strongly related to the monsoon circulations. During the boreal summer when the southwest monsoon prevails, PON is influenced by air masses originating from the

213   Arabian Sea and South India, whereas during the boreal winter, it receives air masses from

214   the east and northeast parts of the Indian subcontinent, and the Bay of Bengal. During the

215   boreal spring and autumn when the monsoon changes its direction, air masses of both origins

216   are observed.

217

218   The Port Blair (PBL) station (11.650 °N, 92.760 °E, 20 m a.s.l.) is located on the small

219   Andaman Islands in the southeastern Bay of Bengal, ~1400 km east of Pondicherry, and

220   roughly 600 km west of Myanmar and Thailand. The station was established in collaboration

221   with the National Institute of Ocean Technology (NIOT), India, and flask air sampling was

222   initiated in July, 2009. The flask sampling inlet is located on the top of a 30 m high tower,

223   and the ambient air is pumped through a Dekabon tubing with a diameter of 1/4". The main

224   city on the Andaman Islands, Port Blair, is about 8 km to the north of the station, with a

225   population of ~100,000 (Census India, 2011). Due to its proximity to vegetation and a small

226   rural community, the station is not completely free from influences of local GHG fluxes.

227   Therefore, flask samples at PBL are obtained in the afternoon between 13:00 and 15:00 LT,

228   when the sea breeze moves towards the land, to minimize significant local influences. Over

229   the period 2009–2011, a total of 63 flask sample pairs were collected at PBL. Back-

230   trajectories show that the air masses sampled at PBL are also controlled by the seasonally

231   reversing monsoon circulations (Fig. 1a), with air masses from the Indian Ocean south of the

232   Equator during the southwest monsoon season, and from the northeast part of the Indian

233   subcontinent, the Bay of Bengal, and Southeast Asia during the northeast monsoon season.

234   As for PON, air masses of both origins are detected at PBL during the boreal spring and

235   autumn when the monsoon changes its direction.

236

2.2 Flask sampling and analysis

2.2.1 Flask sampling

In principle, flask samples are taken in pairs on a weekly basis at all three stations. However, in practice air samples are collected less frequently (on average every 10-12 days) due to bad meteorological conditions or technical problems. Whole air samples are filled into pre-conditioned 1-L cylindrical borosilicate glass flasks (Normag Labor und Prozesstechnik GmbH, Germany) with valves sealed by caps made from KEL-F (PTCFE) fitted at both ends. Besides, a few flasks are equipped with valves sealed by the original Teflon PFA O-ring (Glass Expansion, Australia), accounting for ~5.0, 1.2 and 1.1% of air samples respectively for HLE, PON and PBL during the study period. For the air samples stored in flasks sealed with the original Teflon PFA O-ring, corrections are made for the loss of CO_2 (+0.0027 ppm/day) and of N_2O (+0.0035 ppb/day) after analyses of the samples. The correction factors are empirically determined based on laboratory storage tests using flasks filled with calibrated gases. Drying of the air is performed using 10 g of magnesium perchlorate $(Mg(ClO_4)_2)$ confined at each end with a glass wool plug in a stainless steel cartridge, located upstream of the pump unit. Tests have shown that use of the magnesium perchlorate drier doesn't result in any loss of the target compound. To prevent entrainment of material inside the sampling unit, a 7 μm filter is attached at the end of the cartridge. The flasks are flushed prior to sampling for 10-20 min at a rate of 4–5 L min^{-1}, and the air is compressed in the flasks to about 1 bar over the ambient pressure (pump: KNF Neuberger diaphragm pump powered by a 12V DC motor, Germany, N86KNDC with EPDM membrane). The pressurizing process lasts for less than a minute.

2.2.2 Flask analyses

261 On average the flasks arrive at LSCE, France about 150 days after the sampling date.

262 Leakage could occur during shipment, and any flask sample with too low pressure will be

263 flagged in the analyses. Flask samples are analyzed for CO_2, CH_4, N_2O, SF_6, CO, and H_2 with

264 two coupled gas chromatograph (GC) systems. The first gas chromatograph (HP6890,

265 Agilent) is equipped with a flame ionization detector (FID) for CO_2 and CH_4 detection, and a

266 standard electron capture detector (ECD) for N_2O and SF_6 detection. It is coupled with a

267 second GC equipped with a reduced gas detector (RGD, Peak Laboratories, Inc., California,

268 USA), for analyzing CO and H_2 via reduction of HgO and subsequent detection of Hg vapor

269 through UV absorption. In the following paragraph we summarize the major configurations

270 and parameters of the GC systems (also see Table S1). Further details on the analyzer

271 configuration are described in Lopez (2012) and Yver et al. (2009).

272

273 Both GC systems are composed of three complementary parts: the injection device, the

274 separation elements and the detection sensors. As flask samples are already dried during

275 sampling, they are only passed through a 5 mL glass trap maintained in an ethanol bath kept

276 at -55°C by a cryocooler (Thermo Neslab CC-65) to remove any remaining water vapor. The

277 air samples are flushed with flask overpressure through a 15 mL sample loop for CO_2 and

278 CH_4 analyses, a 15 mL sample loop for N_2O and SF_6 analyses, and a 1 mL sample loop for

279 CO and H_2, at a flow rate of 200 mL min^{-1}. After temperature and pressure equilibration, the

280 air sample is injected into the columns. The CO_2 and CH_4 separation is performed using a

281 Hayesep-Q (12' × 3/16"OD, mesh 80/100) analytical column placed in an oven at 80°C, with

282 a N_2 5.0 carrier gas at a flow rate of 50 ml min^{-1}. Detection of CH_4 and CO_2 (after conversion

283 to CH_4 using a Ni catalyst and H_2 gas) is performed in the FID kept at 250°C. The flame is

284 fed with H_2 (provided by a NM-H_2 generator from F-DBS) at a flow rate of 100 ml min^{-1} and

285 zero air (provided by a 75-82 zero air generator from Parker-Balston) at a flow rate of 300 ml

286 min^{-1}. For N_2O and SF_6 separation, a Hayesep-Q (4' × 3/16" OD, mesh 80/100) pre-column

287 and a Hayesep-Q (6' × 3/16" OD, mesh 80/100) analytical column, both placed in an oven at

288 80°C, are used together with an Ar/CH_4 carrier gas at a flow rate of 40 ml min^{-1}. Detection of

289 N_2O and SF_6 is performed in the ECD heated at 395°C. For CO and H_2, we use a Unibeads

290 1S pre-column (16.5" × 1/8" OD; mesh 60/80) to separate the two gases from the air matrix,

291 and use a Molecular Sieve 5Å analytical column (80" × 1/8" OD; mesh 60/80) to effectively

292 separate H_2 from CO. Both columns are placed in an oven kept at 105°C. CO and H_2 are

293 analyzed in the RGD detector heated to 265°C. A measurement takes ~5 min and calibration

294 gases are measured at least every 0.45 hour. For CO_2, CH_4, N_2O, and SF_6, we use two

295 calibration gases, one with a high concentration and the other with a low concentration. The

296 calibration and quality control cylinders are filled and spiked in a matrix of synthetic air

297 containing N_2, O_2 and Ar prepared by Deuste Steininger (Germany). The concentration of the

298 sample is calculated using a linear regression between the two calibration gases with a time

299 interpolation between the two measurements of the same calibration gas (Messager, 2007;

300 Lopez, 2012). For CO and H_2, we use only one standard and apply a correction for the non-

301 linearity of the analyzer (Yver et al., 2009; Yver, 2010). The nonlinearity is verified regularly

302 with 5 calibration cylinders for CO and 8 calibration cylinders for H_2. All the calibration

303 gases themselves are determined against an international primary scale (CO_2: WMOX2007;

304 CH_4: NOAA2004; N_2O: NOAA2005A; SF_6: NOAA2005; CO: WMOX2004; H_2:

305 WMOX2009; Hall et al., 2007; Dlugokencky et al., 2005; Jordan and Steinberg, 2011; Zhao

306 and Tans, 2006). Finally, a "target" gas is measured every two hours after the calibration

307 gases as a quality control of the scales and of the analyzers. The repeatability of the GC

308 systems estimated from the target cylinder measurements over several days is 0.06 ppm for

309 CO_2, 1 ppb for CH_4, 0.3 ppb for N_2O, 0.1 ppt for SF_6, 1 ppb for CO and 2 ppb for H_2.

310　　Additional quality control is made by checking the values of a flask target (a flask filled with

311　　calibrated gases) placed on each measurement sequence.

312

313　　For both of the GC systems, data acquisition, valve shunting, and temperature regulation are

314　　entirely processed by the Chemstation software from Agilent. Concentrations are calculated

315　　with a software developed at LSCE using peak height or area depending on the species.

316

317　　**2.2.3 Uncertainty of flask measurements**

318　　Uncertainties in the measured concentrations stemmed from both the sampling method and

319　　the analysis. Collecting flask samples in pairs and measuring each flask twice allow us to

320　　evaluate these uncertainties. A large discrepancy between two analyses of the same flask

321　　reveals a problem in the analysis system, while a difference between a pair of flasks reflects

322　　both analysis and sampling uncertainties. Flask pairs with differences in mole fractions

323　　beyond a certain threshold are flagged and rejected (see Table S2 in the supplement for the

324　　threshold for each species). The percentages of flask pairs retained for analyses are 65.9-88.3%

325　　for CO_2, 88.6-94.1% for CH_4, 74.6-91.5% for N_2O, 92.0-96.8% for SF_6, 68.6-88.3% for CO,

326　　and 76.2-95.2% for H_2 (Table S3). For each species, we evaluate the uncertainties by

327　　averaging differences between the two injections of the same flask (analysis uncertainty) and

328　　between the pair of flasks (analysis uncertainty + sampling uncertainty) across all retained

329　　flask pairs from the three Indian stations (Table S4). For all species except SF_6, the sampling

330　　uncertainty turns out to be the major uncertainty, while the analysis uncertainty is equivalent

331　　to the reproducibility of the instrument. For SF_6, both uncertainties are extremely low due to

332　　the small amplitudes and variations of the signals at the three stations.

333

334   At LSCE, there are regular comparison exercises in which flasks are measured by different

335   laboratories on the same primary scale (e.g., Inter-Comparison Project (ICP) loop, Integrated

336   non-CO2 Greenhouse gas Observing System (InGOS) 'Cucumber' intercomparison project).

337   These comparisons allow us to estimate possible biases in our measurements. In Table S4, the

338   bias for each species is calculated over the sampling period using the ICP flask exercise that

339   circulates flasks of low, medium and high concentrations between different laboratories. For

340   CO_2, CH_4, SF_6 and CO, the biases are reported against NOAA (NOAA-LSCE) as it is the

341   laboratory responsible for the primary scales for these species. The bias of H_2 is calculated

342   against Max Planck Institute for Biogeochemistry (MPI-BGC) in Jena, Germany, which is

343   responsible for the primary scale of H_2. The bias of N_2O is reported against MPI-BGC instead

344   of NOAA. Although NOAA is responsible for the primary scale of N_2O, the instruments they

345   use for the N_2O flask analyses and cylinder calibration are not the same as ours. For CH_4,

346   N_2O, SF_6 and H_2, the estimated biases are within the noise level of the instrument and

347   negligible. For CO_2 and CO, we observe a bias of -0.15±0.11 ppm and 3.5±2.2 ppb,

348   respectively (Table S4), which could be due to the nonlinearity of the instrument and/or an

349   improper attribution of the secondary scale values.

350

351   **2.3 Data analyses**

352   **2.3.1 Curve-fitting procedures**

353   For each time series of flask measurements, we calculated annual means and seasonal cycles

354   using a curve-fitting routine (CCGvu) developed by NOAA/CMDL (Thoning et al., 1989). A

355   smoothed function was fitted to the retained data, consisting of a first-order polynomial for

356   the growth rate and two harmonics for the annual cycle (Levin et al., 2002; Ramonet et al.,

357   2002), as well as a low pass filter with 80 and 667 days as short-term and long-term cutoff

358   values, respectively (Bakwin et al., 1998). Residuals were then calculated as the differences

359   between the original data and the smoothed fitting curve. Any data lying outside three

360   standard deviations of the residuals were regarded as outliers and discarded from the time

361   series (Harris et al., 2000; Zhang et al., 2007). This procedure was repeated until no outliers

362   remained. These outliers were likely a result of pollution by local emissions and not

363   representative of regional background concentrations. The data discarded through this

364   filtering procedure accounts for less than 4% of the retained flask pairs after flagging (Table

365   S3). Particularly, for PON where observations can be influenced by local emissions, we also

366   tried to use CO as a tracer and filtered time series of other species by CO outliers. Results

367   show that this additional filtering does not make significant difference to the trends, seasonal

368   cycles and mean annual gradients (relative to HLE) for all the other species at PON (Table S5,

369   Fig. S2). On the other hand, however, the approach may substantially decrease the number of

370   samples used to fit the smooth curve (e.g. ~38% for CH_4) and result in larger data gaps

371   (Table S5, Fig. S2), probably compromising reliability of the analyses. Therefore finally we

372   didn't use CO as a tracer of local emissions for additional filtering.

373

374   For each species at each station, the annual means, as well as the amplitude and phases of

375   seasonal cycles, were determined from the smoothed fitting curve and its harmonic

376   component. We bootstrapped the curve-fitting procedures 1000 times by randomly sampling

377   the original data with replacement to further estimate uncertainties of annual means and

378   seasonal cycles. Since the observation records are relatively short, we used all flask

379   measurements between 2006 and 2011 to fit the smooth curve when available (Fig. S3). For

380   each species, we also compared results with measurements from stations outside India that

381   belong to networks of NOAA/ESRL (http://www.esrl.noaa.gov/gmd/) and Integrated Carbon

382   Observation System (ICOS, https://www.icos-cp.eu/). Locations and the fitting periods of

383   these stations are also given in Table S6, Figs. S1 and S3.

384

385   **2.3.2 Ratio of species**

386   We analyzed CH_4-CO, CH_4-CO_2, and CO-CO_2 correlations using the residuals from the

387   smoothed fitting curves that represent synoptic-scale variations (Harris et al., 2000; Ramonet

388   et al., 2002; Grant et al., 2010). To determine the ratio between each species pair, as in

389   previous studies, we used the slope calculated from the orthogonal distance regression (Press

390   et al., 2007) to equally account for variances of both species (Harris et al., 2000; Ramonet et

391   al., 2002; Schuck et al., 2010; Baker et al., 2012). We also bootstrapped the orthogonal

392   distance regression procedure 1000 times and estimated the 1-σ uncertainty for each ratio.

393   The analyses were performed with R3.1.0 (R Core Team, 2014) following the recipes

394   described in Teetor (2011).

395

396   **3 Results and discussions**

397   **3.1 Annual means and seasonal cycles**

398   **3.1.1 CO_2**

399   Figure 2 shows CO_2 flask measurements and the corresponding smooth curves fitted to the

400   data at HLE, PON and PBL, as well as two additional NOAA/ESRL stations, namely Plateau

401   Assy, Kazakhstan (KZM – 43.25 °N, 77.88 °E, 2519 m a.s.l.) and Waliguan, China (WLG –

402   36.29 °N, 100.90 °E, 3810 m a.s.l.) (Dlugokencky et al., 2014b). HLE observed an increase

403   in CO_2 mole fractions from 382.3±0.3 to 391.4±0.3 between 2007 and 2011, with annual

404   mean values being lower (by 0.2–1.9 ppm) than KZM and WLG (Fig. 2c and d, Table 1). At

405   PON, the annual mean CO_2 mole fractions were generally higher than at HLE, with

406   differences ranging 1.8–4.3 ppm (Fig. 2a, Table 1). The annual mean CO_2 gradient between

407   PON and HLE reflects the altitudinal difference of the two stations, and a larger influence of

408   CO_2 emissions at PON, mostly from South India (Fig. 1a, EDGAR v4.2). Besides this, as

409   shown in Fig. 2a and Table 1, the CO_2 observations at PON are influenced by synoptic scale

410   events, with a large variability of individual measurements relative to the fitting curve (see

411   the relative SDs (RSD) in Table 1). At PBL, the annual mean CO_2 mole fractions were on

412   average 1.2–1.8 ppm lower than that at HLE (Table 1). The negative gradient between PBL

413   and HLE is particularly large during summer, possibly due to clean air masses transported

414   from the ocean (Figs. 1a and 2b). Note that caution should be exercised in interpreting the

415   gradient at PBL because of the data gap and short duration of the time series.

416

417   The different CO_2 seasonal cycles observed at the five stations reflect the seasonality of

418   carbon exchange in the northern terrestrial biosphere as well as influences of long-range

419   transport and the monsoon circulations. At HLE, the peak-to-peak amplitude of the mean

420   seasonal cycle was 8.2±0.4 ppm, with the maximum early May and the minimum mid-

421   September, respectively (Fig. 3, Table 1). The mean seasonal cycle estimated from flask

422   measurements at HLE is in good agreement with that derived from vertical profiles of in-situ

423   aircraft measurements over New Delhi (~500 km southwest of HLE) from the

424   Comprehensive Observation Network for Trace gases by Airliner (CONTRAIL,

425   http://www.cger.nies.go.jp/contrail/) project at similar altitudes (R=0.98–0.99, p<0.001, Fig.

426   3a; Machida et al., 2008), and back-trajectories show that they represent air masses with

427   similar origins as HLE (Fig. S8), confirming that HLE is representative of the regional free

428   mid-troposphere background concentrations. When comparing with the two other background

429   stations located further north in central and East Asia, a significant delay of the CO_2 phase is

430   seen at HLE compared to KZM and WLG (Fig. 3b, Table 1). We also note that the CO_2 mean

431   seasonal cycle at HLE is in phase with the composite zonal marine boundary layer (MBL)

432   reference at 32°N, while for KZM and WLG, an advance in the CO_2 phase by about 1 month

433   is observed compared to the zonal MBL reference (Fig. S4; Dlugokency et al., 2014b). The

434   phase shifts in the CO_2 seasonal cycles mainly result from differences in the air mass origins

435   between stations. HLE is influenced by the long-range transport of air masses from mid-

436   latitudes around 30 °N, as well as air masses passing over the Indian subcontinent in the

437   boreal summer (Fig. 1a), therefore its CO_2 seasonal cycle is related to the seasonality of

438   vegetation activity over the entire latitude band. KZM and WLG receive air masses passing

439   over the Middle East and western Asia as HLE does, but they are also influenced by air

440   masses of more northern origins with signals of strong CO_2 uptake over Siberia during JAS

441   (Fig. S5). At WLG, negative CO_2 synoptic events, indicative of large-scale transport of air

442   masses exposed to carbon sinks in Siberia in summer, were also detected by in-situ

443   measurements during 2009-2011 (Fang et al., 2014). Moreover, the back trajectories indicate

444   that WLG and KZM are more influenced than HLE by air masses that have exchanged with

445   the boundary layer air being affected by vegetation CO_2 uptake (Fig. S6a,d,e). This could

446   additionally account for the earlier CO_2 phase observed at KZM and WLG compared to HLE.

447

448   At PON and PBL, the peak-to-peak amplitudes of the CO_2 mean seasonal cycles were

449   7.6±1.4 and 11.1±1.3 ppm, with their maxima observed in April. The CO_2 mean seasonal

450   cycle is controlled by changes in the monsoon circulations, in combination with the

451   seasonality of CO_2 biotic exchange and anthropogenic emissions in India. During the boreal

452   winter when the NE monsoon prevails, PON and PBL receive air masses enriched in CO_2

453   from the East and Northeast Indian subcontinent as well as from Southeast Asia, with large

454   anthropogenic CO_2 emissions (EDGAR v4.2; Wang et al., 2013; Kurokawa et al., 2013).

455   During April when the SW monsoon begins to develop, the two stations record a decrease in

456 CO_2 because of the arrival of air masses depleted in CO_2 originating from the Indian Ocean

457 south of the Equator (Fig. 1a, Fig. 3c). Compared to PBL, the CO_2 decrease at PON is less

458 pronounced and longer, probably because of the influence of anthropogenic emissions in

459 South India. The CO_2 mean seasonal cycle at PON is also similar to that observed at CRI

460 (15.08°N, 73.83°E, 60m a.s.l.), another station on the southwest coast of India, yet the

461 seasonal maximum at CRI is reached slightly earlier than at PON in March (Bhattacharya et

462 al., 2009; Tiwari et al., 2011, 2014). The SNG station (18.35°N, 73.75°E, 1600m a.s.l.),

463 located over the Western Ghats, observes a larger CO_2 seasonal cycle with a peak-to-peak

464 amplitude of ~20 ppm (Tiwari et al., 2014).

465

466 **3.1.2 CH_4**

467 Figure 4 presents the time series of CH_4 flask measurements at the three Indian stations and

468 the two NOAA/ESRL stations (Dlugokencky et al., 2014a), with their corresponding

469 smoothed curves for 2007–2011. At HLE, the annual mean CH_4 concentration increased from

470 1814.8±2.9 to 1849.5±5.2 ppb between 2007 and 2011 (Fig. 4, Table 1). The multiyear mean

471 CH_4 value at HLE was lower than at KZM and WLG by on average 25.7±3.1 and 19.6±7.8

472 ppb (Fig. 4c and d, Table 1), respectively, reflecting the latitudinal and altitudinal CH_4

473 gradients. Indeed, KZM and WLG receive air masses transported from Siberia with large

474 wetland CH_4 emissions in summer, as well as those from regional sources closer to the

475 stations (Fang et al., 2013; Fig. S5), which may further contribute to the positive gradients

476 between these two stations and HLE. At PON and PBL, the annual mean CH_4 mole fractions

477 were higher than those at HLE by as much as 37.4±10.7 and 19.8±24.5 ppb respectively (Fig.

478 4a and b, Table 1). The positive gradients indicate significant regional CH_4 emissions,

479 especially during winter when the NE monsoon transports air masses from East and

480 Northeast India and Southeast Asia, where emissions from livestock, rice paddies and a

481 variety of waterlogged anaerobic sources and residential biofuel burning are high (EDGAR

482 v4.2; Baker et al., 2012; Kurokawa et al., 2013). The in-situ measurements at Darjeeling,

483 India (27.03°N, 88.25°E, 2194 m a.s.l.), another station located in the eastern Himalayas, also

484 showed large variability and frequent pollution events in CH_4 mole fractions, which largely

485 result from the transport of CH_4-polluted air masses from the densely populated Indo-

486 Gangetic Plains to the station (Ganesan et al., 2013).

487

488 The CH_4 seasonal cycles exhibit contrasting patterns across stations. As shown in Fig. 5, a

489 distinct characteristic of the mean seasonal cycle at HLE is a CH_4 maximum from June to

490 September. Even KZM and WLG do not show a minimum in summer that would be

491 characteristic for the enhanced CH_4 removal rate by reaction with OH. The pronounced HLE

492 feature is consistent with the result from the aircraft flask measurements over India at flight

493 altitudes of 8–12.5 km by the Civil Aircraft for the Regular Investigation of the atmosphere

494 Based on an Instrument Container (CARIBIC, http://www.caribic-atmospheric.com/) project

495 (Schuck et al., 2010, 2012; Baker et al., 2012), although a larger seasonal cycle amplitude is

496 found in the CARIBIC composite data due to the rapid vertical mixing over the monsoon

497 region and the strong anticyclone that develops in the upper troposphere (Fig. 5a; Schuck et

498 al., 2010). CARIBIC sampled the mid- to upper tropospheric air masses that were earlier and

499 more strongly enriched in CH_4, as a result of the rapid vertical transport of surface air masses

500 by deep convection and subsequent accumulation and confinement of pollutants within the

501 strong, closed circulation of the anticyclone (Li et al., 2005; Randel and Park, 2006). Xiong et

502 al. (2009) also reported enhancements of CH_4 during the summer monsoon season over South

503 Asia based on satellite retrievals of CH_4 using the Atmospheric Infrared Sounder (AIRS) on

504 the EOS/Aqua platform as well as model simulations. Moreover, the mean CH_4 seasonal

505 cycle at HLE agrees well with the seasonal variations of CH_4 emissions from wetlands and

506   rice paddies and convective precipitation over the Indian subcontinent (Fig. 5b), suggesting

507   that the summer maximum at HLE are likely related to the enhanced biogenic CH_4 emissions

508   from wetlands and rice paddies and deep convection that mixes surface emissions into the

509   mid-to-upper troposphere. During the SW monsoon period (June–September), convection

510   over the Indian subcontinent and the Bay of Bengal rapidly mixes surface polluted air with

511   the upper troposphere, therefore concentrations of trace gases would be enhanced at higher

512   altitudes rather than at the surface (Schuck et al., 2010; Lawrence and Lelieveld, 2010).

513   Further analyses of carbon isotopic measurements and/or chemical transport model are

514   needed to disentangle and quantify the contributions of meteorology and biogenic emissions

515   to the CH_4 summer maximum at HLE. As stated above, KZM and WLG also record CH_4

516   increases during summertime, but with smaller magnitudes (Fig. 5a), possibly because they

517   are not directly influenced by deep convection from the Indian monsoon system.

518

519   In contrast to HLE, the CH_4 mean seasonal cycles at PON and PBL have distinct phases and

520   much larger amplitudes, with minimum CH_4 values during July (Fig. 5c). These not only

521   reflect higher rates of removal by OH, but rather the influence of southern hemispheric air

522   transported at low altitudes from the southwest as well as the dilution effect by increased

523   local planetary boundary layer height. In boreal winter, the maxima at PON and PBL are

524   associated with CH_4-enriched air masses transported from East and Northeast India, and

525   Southeast Asia, mostly polluted by agricultural-related sources (e.g., livestock, rice paddies,

526   agricultural waste burning). As PON and PBL, the flask measurements at CRI also showed

527   the seasonal maximum CH_4 values during the NE monsoon season, reflecting influences of

528   air masses with elevated CH_4 from the Indian subcontinent (Bhattacharya et al., 2009; Tiwari

529   et al., 2013).

530

3.1.3 N_2O

Nitrous oxide (N_2O) is a potent greenhouse gas that has the third largest contribution to anthropogenic radiative forcing after CO_2 and CH_4 (IPCC, 2013). It also becomes the dominant ozone depleting substance (ODS) emitted in the 21st century with the decline of chlorofluorocarbons (CFCs) under the Montreal Protocol (Ravishankara et al., 2009). Since the pre-industrial era, the atmospheric N_2O increased rapidly from ~270 ppb to ~325 ppb in 2011 (IPCC, 2013), largely as the result of human activities. Of the several known N_2O sources, agricultural activities (mainly through nitrogen fertilizer use) contribute to ~58% of the global anthropogenic N_2O emissions, with a higher share in a predominantly agrarian country like India (~75%; Garg et al., 2012).

The time series of N_2O flask measurements over the period of 2007–2011 and their smoothed curves are presented in Fig. 6. At HLE, the annual mean N_2O concentration rose from 322.2±0.1 to 325.2±0.1 ppb during 2007–2011 (Table 1), with a mean annual growth rate of 0.8±0.0 ppb yr^{-1} (r^2 = 0.97, p = 0.001), smaller than that at MLO (1.0±0.0 ppb yr^{-1}, Table 1). At PON and PBL, the annual mean N_2O mole fractions are higher than at HLE by 3.1±0.3 and 3.8±1.7 ppb (Fig. 6, Table 1), respectively. The N_2O gradients between PON, PBL and HLE are larger than typical N_2O gradients observed between stations scattered in Europe or in North America. For example, Haszpra et al. (2008) presented N_2O flask measurements at a continental station – Hegyhátsál, Hungary (HUN – 46.95 °N, 16.65 °W, 248 m a.s.l.) from 1997 to 2007. The annual mean N_2O mole fraction at HUN was higher than at Mace Head (MHD) by only 1.3 ppb. We also analyzed N_2O time series of flask measurements during 2007–2011 at several European coastal stations – BGU in Spain, FIK in Greece, and LPO in France (Table S6), and the N_2O gradients between these stations and MHD were 1.1±0.2, 0.4±0.1, and 2.1±0.6 ppb, respectively (Fig. S10, Table S7). In the United States, N_2O flask

556 measurements from the NOAA/ESRL stations at Park Falls, Wisconsin (LEF – 45.95 °N,

557 90.27 °W, 472 m a.s.l.), Harvard Forest, Massachusetts (HFM – 42.54 °N, 72.17 °W, 340 m

558 a.s.l.) and a continental, high-altitude station at Niwot Ridge, Colorado (NWR – 40.05 °N,

559 105.58 °W, 3523 m a.s.l.) also show that, the annual mean N_2O concentrations at HFM and

560 LEF were higher than that at NWR by only 0.5±0.1 and 0.3±0.1 ppb, respectively (Fig. S10,

561 Table S7). Besides, the N_2O concentrations measured at PON and PBL have a notably higher

562 variability (around the smoothed fitting curve) than that at European and US stations (see

563 relative SDs (RSD) in Table 1 and Table S7). The larger N_2O gradient between PON, PBL

564 and HLE, as well as higher variability at PON and PBL, demonstrate the presence of

565 substantial N_2O sources in South Asia and over the Indian Ocean during the observation

566 period. The in-situ measurements at Darjeeling also exhibited N_2O enhancements to be above

567 the background level, suggesting significant N_2O sources in this region (Ganesan et al., 2013).

568 These sources may be related to emissions from natural and cultivated soils probably

569 enhanced by extensive use of nitrogen fertilizers, as well as emissions from regions of coastal

570 upwelling in the Arabian Sea (Bange et al., 2001; Garg et al., 2012; Saikawa et al., 2014).

571

572 Compared to CO_2 and CH_4, the seasonal cycle of N_2O is very small due to the long lifetime

573 of ~120 years (Minschwaner et al., 1993; Volk et al., 1997), and has a larger uncertainty

574 probably because synoptic events are more likely to mask the seasonal signal. At HLE, PON

575 and PBL, the peak-to-peak amplitudes of the N_2O seasonal cycle are 0.6±0.1, 1.2±0.5, and

576 2.2±0.6 ppb, respectively (Table 1). HLE displays a N_2O maximum in mid-August (Student's

577 t-test, t=1.78, p=0.06), and a secondary maximum is in January/February but not significant

578 (Student's t-test, t=-0.84, p=0.79) (Table 1, Fig. 7, Table S8 for detailed t-test statistics). The

579 N_2O seasonal cycle at HLE is out of phase with that at other northern background stations

580 such as MHD (Fig. S11, Table S7), where an N_2O summer minimum is always observed,

581   likely due to the downward transport of N_2O-depleted air from the stratosphere to the

582   troposphere during spring and summer (Liao et al., 2004; Morgan et al., 2004; Jiang et al.,

583   2007b). The timing of the summer N_2O maximum at HLE is consistent with that of CH_4

584   (Table 1; Figs. 5 and 7), giving evidence that the N_2O seasonal cycle may probably be

585   influenced by the convective mixing of surface air, rather than by the influx of stratospheric

586   air into the troposphere. Given that the populous Indo-Gangetic plains have high N_2O

587   emission rates due to the intensive use of nitrogen fertilizers (Garg et al., 2012; Thompson et

588   al., 2014a), during summer, the surface air enriched in N_2O is vertically transported by deep

589   convection and enhances N_2O mole fractions in the mid-to-upper troposphere. Like CH_4, the

590   N_2O enhancement during the summer monsoon period (June-September) was also observed

591   by the aircraft flask measurements at flight altitudes 8–12.5 km from the CARIBIC project in

592   2008 (Schuck et al., 2010).

593

594   At PON, N_2O also decreases during February–April and reaches a minimum at the end of

595   May. However, the decrease of N_2O does not persist during June–September, which is in

596   contrast with CH_4 (Table 1, Fig. 7a). One reason may be that the air masses arriving at the

597   site during the southwest monsoon period is relatively enriched in N_2O compared to CH_4,

598   reflecting differences in their relative emissions along the air mass route. The increase of N_2O

599   at PON during June–August and the maximum during September–October are likely related

600   to N_2O emissions from coastal upwelling along the southern Indian continental shelf, which

601   peak during the SW monsoon season (Patra et al., 1999; Bange et al., 2001). According to

602   Bange et al. (2001), the annual N_2O emission for the Arabian Sea is 0.33–0.70 Tg/yr, of

603   which N_2O emissions during the SW monsoon account for about 64–70%. This coastal

604   upwelling N_2O flux is significantly larger than the annual anthropogenic N_2O emissions in

605   South India south of 15 °N, which is estimated to be on average 0.07–0.08 Tg/yr during

606   2000–2010 (EDGAR v4.2). At PBL, the maximum and minimum N_2O occur in November

607   and February/March, respectively (Table 1, Fig. 7b). The late N_2O peak at PBL in November

608   may be associated with the N_2O-enriched air masses transported from South and Southeast

609   Asia, which could be attributed to natural and agricultural N_2O emissions from this region

610   (Saikawa et al., 2014). It should be noted that, the mean seasonal cycles of N_2O at PON and

611   PBL are subject to high uncertainties because of the short observation periods and data gaps

612   (shaded area in Fig. 7). The N_2O maximum and/or minimum obtained from the mean

613   seasonal cycle are marginally significant for PON and PBL (Table S8 for detailed t-test

614   statistics). Therefore, caution should be exercised in interpreting mean seasonal cycles at

615   these stations. Sustained, long-term measurements are needed in order to generate more

616   reliable estimates of the seasonal cycles for the two stations.

617

618   **3.1.4 SF_6**

619   Sulfur hexafluoride (SF_6) is an extremely stable greenhouse gas, with an atmospheric lifetime

620   as long as 800–3200 year and a global warming potential (GWP) of ~23,900 over a 100-year

621   time horizon (Ravishankara et al., 1993; Morris et al., 1995; IPCC, 2013). The main sources

622   of atmospheric SF_6 emissions are electricity distribution systems, magnesium production, and

623   semi-conductor manufacturing (Olivier et al., 2005), while its natural sources are negligible

624   (Busenberg and Plummer, 2000). As its sources are almost purely anthropogenic (Maiss et al.,

625   1996), SF_6 is widely considered as a good tracer for population density, energy consumption

626   and anthropogenic GHG emissions (Haszpra et al., 2008).

627

628   Figure 8 presents the time series of SF_6 flask measurements and corresponding fitting curves

629   at HLE, PON, and PBL. At HLE, the annual mean SF_6 mole fractions increased from

630   6.26 ± 0.03 to 7.38 ± 0.01 ppt between 2007 and 2011, which is in good agreement with the SF_6

631   trend observed at MLO during the same period (HLE: 0.29 ± 0.05 ppt/yr, r^2=0.99, p<0.001;

632   MLO: 0.29 ± 0.03 ppt/yr, r^2=0.99, p<0.001; Figs. 8 and S12a, Table 1, Table S9). The annual

633   mean SF_6 gradient between PON and HLE is -0.060 ± 0.030 ppt, whereas the gradient between

634   PBL and HLE is statistically insignificant (-0.002 ± 0.097 ppt). The slight negative gradient

635   between PON and HLE is a reversed signal compared with the SF_6 observations at stations

636   influenced by continental emissions in Europe and United States. For example, the SF_6 mole

637   fractions at HUN over the years of 1997–2007 are higher than those at MHD by on average

638   0.19 ppt (Haszpra et al., 2008). We also analyzed the SF_6 gradients between two coastal

639   European stations – BGU (41.97 °N, 3.3 °E, 30 m a.s.l.) and LPO (48.80 °N, 3.57 °W, 30 m

640   a.s.l.) – and MHD, which are 0.10 ± 0.03 and 0.05 ± 0.02 ppt averaged over the period of 2007–

641   2011, respectively. At HFM, the SF_6 mole fractions are higher than those of the NWR on

642   average by 0.15 ± 0.06 ppt during 2007–2011 (Table S9). Given the long atmospheric lifetime

643   of SF_6, the positive gradients between continental European and US stations and background

644   reference stations suggest significant sources in Europe and the US. On the contrary, the

645   slight negative gradient between PON and HLE implies weak SF_6 emissions over the Indian

646   subcontinent, which is also indicated by recent high-frequency in-situ SF_6 measurements at

647   Darjeeling (Ganesan et al., 2013). It is also worthwhile to note that high SF_6 values occur

648   repeatedly at HLE and PBL in winter, which is likely related to episodic SF_6 pollution events

649   from the Middle East, South/Southeast Asia and China (Figs. 8b and S7d).

650

651   The annual mean SF_6 seasonal cycles for HLE, PON, and PBL are presented in Fig. 9. The

652   peak-to-peak amplitudes at the three stations are 0.15 ± 0.03, 0.24 ± 0.02, and 0.48 ± 0.07 ppt,

653   respectively (Table 1). At HLE, the SF_6 seasonal cycle is bimodal as for N_2O, with an

654   absolute maximum occurring in November (Student's t-test, t=2.425, p=0.014) and a

655 secondary maximum in May (Student's t-test, t=2.443, p=0.016) (Table S10 for detailed t-test

656 statistics). Given that SF_6 increases monotonously and that its sources are purely

657 anthropogenic and not subject to seasonally variations (Maiss et al., 1996), the seasonal cycle

658 of SF_6 should be driven by changes in atmospheric circulations, e.g., the SW monsoon

659 convection and stratosphere-atmosphere exchange (Levin et al., 2002). We note that, at HLE,

660 no enhancement of SF_6 during the SW monsoon season is recorded, unlike what is observed

661 for CH_4 and N_2O (Figs. 5 and 7). Although the CARIBIC aircraft flask measurements over

662 the Indian region demonstrated SF_6 enhancements in the upper troposphere at ~30 °N

663 (approximately where HLE is located) in August, 2008, they are not related to the deep

664 convection and surface sources that contribute to the summer maxima in CH_4 and N_2O. Back-

665 trajectories from the CARIBIC flights showed that the summer enhancements in SF_6 were

666 related to air samples collected north of 20°N along the flight routes, where air masses were

667 more influenced by the westerly subtropical jet (and a smaller anticyclone embedded in it

668 over the Arabian Peninsula) rather than the deep convection in the monsoon region

669 (Krishnamurti et al. 2008; Schuck et al., 2010; Fig. S9). Since HLE is not influenced by the

670 westerly subtropical jet in the upper troposphere (also clearly seen by the colors of back-

671 trajectories in Fig. S9), the summer enhancements of SF_6 observed by the CARIBIC flights

672 are not detected by the flask measurements at HLE. The absence of SF_6 enhancement in

673 summer at HLE confirms weak SF_6 emissions in India. At PBL, the SF_6 seasonal cycle is

674 related to the monsoon circulation and convection (Figs. 9b and S7d). The maximum during

675 November–December (Student's t-test, t=5.138, p<0.001; Table S10) is likely due to frequent

676 episodic SF_6 polluted air masses transported from Southeast Asia and China (Fig. S7d).

677

678 **3.1.5 CO**

679   Carbon monoxide (CO) plays important roles in atmospheric chemistry, as the dominant sink

680   for the hydroxyl radical (OH, the main tropospheric oxidant) and a precursor of tropospheric

681   ozone under high NO_x ($NO+NO_2$) concentrations (Logan et al., 1981; Novelli et al., 1998;

682   Seinfeld and Pandis, 2006). Although CO does not act as a greenhouse gas, it modulates the

683   atmospheric concentrations of CH_4 (the second anthropogenic greenhouse gas after CO_2)

684   through competition for the OH radicals. At the global scale, it contributes to an indirect

685   positive radiative forcing of $0.23\pm0.07Wm^{-2}$ (IPCC, 2013). Besides, CO is an excellent tracer

686   for combustion processes, with emission sources mainly contributed by incomplete

687   combustion of fossil fuel and biofuels, and by biomass burning (Granier et al., 2011). In India,

688   biofuel and agricultural waste burning account for 70–80% of the total anthropogenic CO

689   emissions (EDGAR v4.2; Streets et al., 2003b; Yevich and Logan, 2003).

690

691   The time series of CO flask measurements and corresponding smoothed curves are shown in

692   Fig. 10. Over the period of 2007–2011, HLE recorded a slight decrease in CO mole fractions

693   from 104.7 ± 1.4 to 99.4 ± 2.2 ppb, with an annual rate of -2.2 ± 0.0 ppb yr^{-1} ($r^2 = 0.65$, p = 0.06).

694   The CO mole fractions at HLE are lower than those at KZM and WLG (Novelli et al., 2014b),

695   by on average 18.8 ± 2.5 and 30.2 ± 7.4 ppb, respectively (Table 1, Fig. 10c and d). The

696   positive gradient between KZM, WLG and HLE does not only reflect decreasing CO with

697   altitude and the N-S global gradient, but also suggests differences in regional emission

698   sources. For example, compared to HLE, the CO signals at WLG are more influenced by

699   transport of polluted air, especially during summer when about 30% air masses pass over

700   industrialized and urbanized areas southeast of the station (Zhang et al., 2011). Besides, the

701   positive CO gradient between KZM, WLG and HLE may be further contributed by air

702   masses of northern Siberia origin in summer (Fig. S5), with higher CO emissions from

703   biomass burning and secondary CO from the oxidation of CH_4 and non-CH_4 hydrocarbons

704   (Konovalov et al., 2014). At PON and PBL, the annual mean CO mole fractions are higher

705   than that at HLE by on average 82.4±10.7 and 52.5±8.5 ppb, respectively (Table 1, Fig. 10a

706   and b). The PON and PBL stations are influenced by CO regional emissions, mainly due to

707   biofuel and agricultural burning over South and Southeast Asia (Lelieveld et al., 2001; Streets

708   et al., 2003a, b; Yevich and Logan, 2003). We also note that, for all the five stations, the CO

709   time series show larger variability with respect to their corresponding smoothed curves than

710   other species do (see the residual SD (RSD) in Table 1, Fig. 10), as a result of the unevenly

711   distributed CO sources and short atmospheric lifetime (Novelli et al., 1992).

712

713   As shown in Fig. 11, the CO seasonal cycle at HLE reaches a maximum in mid-March and a

714   minimum by the end of October, with a peak-to-peak amplitude of 28.4±2.3 ppb (Table 1,

715   Fig. 11). The phase of the mean CO seasonal cycle at HLE generally agrees with the ones

716   observed at KZM and WLG, with a lag of up to 1 month in the timing of seasonal minimum

717   at the two stations (Table 1, Fig. 11c and d). In contrast with the three stations representative

718   of large-scale free tropospheric air masses, the stations at the maritime boundary layer in the

719   mid-to-high Northern Hemisphere observe the lowest CO values in July or August (Novelli et

720   al., 1992, 1998), when the concentration of OH – the major sink of CO – is highest (Logan et

721   al., 1981). The delay in timing of the seasonal CO minimum at the three free troposphere

722   stations in Central and South Asia compared to those boundary layer stations is probably due

723   to the mixing time of regional surface CO emissions and the relatively short lifetime of CO

724   (1-2 months on average). During summer, KZM and WLG sample air masses from Siberia

725   impacted by CO fire emissions (Duncan et al., 2003; Kasischke et al., 2005), as well as CO-

726   polluted air from urbanized and industrialized area (Zhang et al., 2011), while HLE is

727   influenced by convective mixing of CO emissions from India, either from anthropogenic

728   sources or oxidation of VOCs. It is interesting to note that the CO seasonal cycle at HLE does

729 not show an enhancement during JAS as CH_4 and N_2O do (Figs. 5 and 7), possibly as a result

730 of OH oxidation that reduces CO and acts oppositely to vertical transport, and/or differences

731 in seasonal emission patterns between CO and the other two species (Baker et al., 2012).

732 However, the CO enhancement during summer was observed in the upper troposphere over

733 South Asia from the CARIBIC aircraft measurements at flight altitudes 8-12.5 km and

734 Microwave Limb Sounder observations at 100–200 hPa (Li et al., 2005; Jiang et al., 2007a;

735 Schuck et al., 2010). The differences in the CO seasonal cycles at different altitudes suggest

736 faster transport (and younger air masses) at 10 km than at 5 km due to convection, controlling

737 the vertical profile of CO, which makes it difficult to directly compare aircraft measurements

738 in the upper troposphere and column remote sensing observations with surface data.

739

740 At PON and PBL, the mean CO seasonal cycles show maxima in the boreal winter and

741 minima in the boreal summer, with peak-to-peak amplitudes of 78.2±11.6 and 144.1±16.0

742 ppb, respectively (Fig. 11a and b). A strong and positive correlation is found between

743 detrended CO and CH_4 at PON (r=0.70, p<0.001) and PBL (r=0.84, p<0.001), suggesting that

744 the seasonal cycles of both species are dominated by the seasonally varying atmospheric

745 transport. During summer when the southwest monsoon prevails, the surface CO

746 concentrations at PON and PBL are low due to rapid convective uplifting and advection of

747 clean air masses from the ocean. During winter, the two stations are influenced by

748 northeasterly air masses enriched in CO from Northeast India, Southeast Asia and China

749 (back-trajectories in Fig. S7e), probably influenced by biofuel and agricultural waste burning

750 in these regions (Yevich and Logan, 2003; Lelieveld et al., 2001).

751

752 **3.1.6 H_2**

753 Hydrogen (H_2) is the second most abundant reduced trace gas in the troposphere after CH_4,

754 with an average mole fraction of ~530 ppb (Novelli et al., 1999). It plays important roles in

755 tropospheric and stratospheric chemistry and indirectly impacts budgets of CH_4, CO and non-

756 methane hydrocarbons (NMHCs) through reaction with the OH radicals (Novelli et al., 1999;

757 Ehhalt and Rohrer, 2009). Like CO, H_2 is also a good tracer for incomplete combustion

758 emissions from fossil fuel and biomass/biofuel burning, which is quite extensive in India

759 (Streets et al., 2003b; Yevich and Logan, 2003).

760

761 Figure 12 shows the time series of H_2 flask measurements with smoothed curves at HLE,

762 PON, and PBL, respectively. No significant trend was observed at any of the three stations

763 (Table 1, Fig. 12), consistent with the long-term H_2 measurements at other background

764 stations during the last three decades (Novelli et al., 1999; Ehhalt and Rohrer, 2009; Grant et

765 al., 2010). For the year 2008, comparing to KZM and WLG (Novelli et al., 2014a), HLE

766 recorded higher H_2 mole fractions by ~40 ppb, reflecting the latitudinal gradient of H_2 with

767 lower concentrations towards northern high latitudes, due to land uptake by soils (Novelli et

768 al., 1999; Price et al., 2007; Hauglustaine and Ehhalt, 2002; Ehhalt and Rohrer, 2009). Note

769 that these results based on only one-year comparison need to be confirmed by extended data

770 more up-to-date, which are not available yet. At PON and PBL, the annual mean H_2 mole

771 fractions were higher than at HLE by 29.8±4.1 and 21.8±4.6 ppb, respectively (Table 1; Fig.

772 12). Comparisons with H_2 measurements at Mariana Island, Guam (GMI – 13.39 °N,

773 144.66 °E, 0.00 m a.s.l.) (Novelli et al., 2014a), another maritime station in the western

774 Pacific at a similar latitude as PON and PBL, also showed positive gradients of ~40 ppb (Fig.

775 S13c and d; Table S11), suggesting substantial regional H_2 sources over the footprint area of

776 PBL and PON. During October–March when the NE monsoon prevails, both PON and PBL

777 receive H_2-enriched air masses from South and Southeast Asia, mainly influenced by fossil

778 fuel combustion and biomass burning (Fig. S7f; GFED v3.1; Hauglustaine and Ehhalt, 2002;

779 Price et al., 2007; Ehhalt and Rohrer, 2009; van der Werf et al., 2010). During April–

780 September, with the northward movement of Intertropical Convergence Zone (ITCZ), the two

781 stations are influenced by advection of air from south of the Equator. For PON, H_2-polluted

782 air masses are occasionally sampled during JAS when the SW monsoon moves over the

783 continent of South India with high population and heavy industry (Fig. S7f; Census India,

784 2011).

785

786 The mean H_2 seasonal cycles for HLE, PON, and PBL are presented in Fig. 13. At HLE, the

787 peak-to-peak H_2 seasonal amplitude is 15.8±2.2 ppb, less than half of the seasonal amplitudes

788 at BMW (39.6±2.6 ppb) and MID (38.0±2.4 ppb) of similar latitudes (Novelli et al., 2014a),

789 and that at WLG (22.8±3.0 ppb) (Figs. 13d and S14a, Tables 1 and S11). The maximum and

790 minimum of H_2 occur in April and September, respectively. The dampening of the H_2

791 seasonal amplitude with increasing altitude was previously found for another high-altitude

792 continental station at Jungfraujoch, Switzerland (JUN – 46.53 °N, 7.98 °E, 3580.00 m a.s.l.)

793 (Bond et al., 2011), and was also captured by the GEOS-Chem global chemical transport

794 model (Price et al., 2007). Since the soil sink dominates much of the surface H_2 seasonal

795 cycle in the mid-to-high Northern Hemisphere (Hauglustaine and Ehhalt, 2002; Price et al.,

796 2007; Bousquet et al., 2011; Yver et al., 2011; Yashiro et al., 2011), the smaller amplitude in

797 the H_2 seasonal cycle at HLE may be attributed to the weakened soil sink with increasing

798 altitude due to vertical mixing (Price et al., 2007; Bond et al., 2011).

799

800 At PON and PBL, the mean H_2 seasonal cycles are characterized by the peak-to-peak

801 amplitudes of 21.6±3.4 and 21.3±5.0 ppb respectively, comparable to that at GMI (21.5±1.2

802   ppb) (Tables 1 and S11, Figs. 13a and b and S14b). At PBL, the H_2 maximum in March–

803   April and a secondary increase during September–October coincide with the double biomass

804   burning peaks in each hemisphere – in March for northern tropics, in August/September for

805   southern tropics (van der Werf et al., 2006; Price et al., 2007; Bousquet et al., 2011; Yver et

806   al., 2011). Given that the seasonal variation of soil H_2 uptake is probably small in the tropics

807   (Price et al., 2007; Bousquet et al., 2011; Yver et al., 2011; Yashiro et al., 2011), this bimodal

808   H_2 seasonal cycle at PBL could be related to biomass burning.

809

810   **3.2 Synoptic variations**

811   In this section we analyze synoptic variations of CO_2, CH_4, and CO by examining

812   correlations between species, after subtracting the smoothed curve from the original data.

813   Ratios of trace gas mole fractions or their enhancements have been widely used in previous

814   studies to partition contributions from different source types and origins (Langenfelds et al.,

815   2002; Paris et al., 2008, Lopez et al., 2012), to estimate emissions of one species given

816   emissions of another one that is better-known (Gamnitzer et al., 2006; Rivier et al., 2006;

817   Turnbull et al., 2006; Schuck et al., 2010), and to provide valuable constraints on inversion of

818   sources and sinks of trace gases (Xiao et al., 2004; Pison et al., 2009).

819

820   **3.2.1 $\Delta CH_4/\Delta CO$**

821   Figure 14 shows scatterplots of CH_4 and CO residuals with the orthogonal distance regression

822   lines at HLE, PON, and PBL for different seasons. A significant and positive correlation

823   between CH_4 and CO residuals (hereafter $\Delta CH_4/\Delta CO$, unit ppb ppb^{-1}) is found for all three

824   stations throughout the year. Furthermore, the $\Delta CH_4/\Delta CO$ ratio also shows seasonal variation

825   at each of the three stations. The most prominent feature is the occurrence of maximum

826   slopes in July–September (also October–December at PON), especially at HLE and the

827   generally higher ratios at this station. Wada et al. (2011) and Niwa et al. (2014) also reported

828   increased summer $\Delta CH_4/\Delta CO$ over the western North Pacific, according to the in-situ

829   measurements at several surface stations and aircraft flask measurements in the mid-

830   troposphere. The main process for this seasonal variation of $\Delta CH_4/\Delta CO$ might be the

831   enhanced emissions of biogenic CH_4 in summer (e.g., wetland and rice paddy emissions;

832   Streets et al., 2003a;Yan et al., 2003) combined with concurrent lower anthropogenic CO

833   emissions in summer than in winter (due to less residential fuel use for heating, see Streets et

834   al., 2003a). The faster photochemical destruction of CO by increased OH during summer

835   cannot explain such large changes (less than 15% according to Wada et al. (2011)).

836

837   At HLE, the $\Delta CH_4/\Delta CO$ ratio varies from 1.2±0.3 to 4.0±1.2 ppb ppb^{-1} throughout the year,

838   with a maximum in JAS, corresponding to the summer monsoon season (Fig. 14a-d). Based

839   on the CARIBIC flights between 10 and 12 km from Frankfurt, Germany to Chennai, India,

840   Baker et al. (2012) derived a $\Delta CH_4/\Delta CO$ ratio in the range 1.88(±0.22) to 4.43(±0.56) in JAS

841   over South Asia. The maximum $\Delta CH_4/\Delta CO$ observed during summer in the mid-to-upper

842   troposphere may be the result of higher biogenic CH_4 emission over the Indian subcontinent,

843   lower CO emissions, combined with frequent widespread convective uplift of surface air

844   during the SW monsoon (Schuck et al., 2010; Baker et al., 2012). The CARIBIC flights

845   recorded similar $\Delta CH_4/\Delta CO$ values to HLE, confirming that convection plays a dominant

846   role compared to advection during the SW monsoon season. Outside the SW monsoon season,

847   both the CARIBIC flights and HLE do generally not record strong effects of surface

848   emissions due to the weakened vertical transport. With respect to the $\Delta CH_4/\Delta CO$ ratios for

849   January–March, April–June and October–December, our estimates are 1.5 to 4 times that of

850   the ratios determined for air masses with signatures of fossil fuel combustion, according to

851   several aircraft and ground observations in East and Southeast Asia (Table S12; Sawa et al.,

852   2004; Lai et al., 2010; Wada et al., 2011; Niwa et al., 2014), which rules out fossil fuel

853   combustion as an explanation for the higher ratios. Our ratios are comparable to the

854    $\Delta CH_4/\Delta CO$ values inferred for air masses of Siberian origin during winter (Table S12; Harris

855   et al., 2000; Chi et al., 2013), and we also obtain similar estimates of $\Delta CH_4/\Delta CO$ from the

856   flask measurements at KZM over the study period (The $\Delta CH_4/\Delta CO$ ratios for KZM are

857   0.8±0.2, 1.7±0.2 and 1.5±0.3 ppb ppb^{-1} for AMJ, OND and JFM, respectively), which are

858   influenced by air masses originating from North Africa, the Middle East, and Central Asia as

859   seen at HLE (see back-trajectories in Fig. S5). Given that oil and gas production accounts for

860   50–70% of CH_4 emissions in these regions (EDGAR v4.2) and that over dry areas the

861   daytime boundary layer is higher which favors injection of surface emissions into the

862   troposphere, the preferential enrichment in CH_4 relative to CO at HLE may tentatively be

863   attributed to fossil CH_4 emissions over gas extraction regions and transported eastwards by

864   westerlies (Harris et al., 2000; Tohjima et al., 1996).

865

866   At PON and PBL, the $\Delta CH_4/\Delta CO$ ratios are in general considerably higher than 0.3 for all

867   seasons, putting them in the range of ratios indicative of urban/industrial sources (Table S12;

868   Harriss et al., 1994; Sawa et al., 2004; Xiao et al., 2004; Bakwin et al., 1995; Lai et al., 2010;

869   Wada et al., 2011; Niwa et al., 2014). However, this does not rule out contributions from

870   biomass/biofuel burning with emissions having a typical $\Delta CH_4/\Delta CO$ ratio less than 0.3

871   (Mauzerall et al., 1998; Andreae and Merlet, 2001; Mühle et al., 2002). Considering that

872   biofuel and agriculture waste burning are the primary energy sources in rural India (Streets et

873   al., 2003a; Yevich and Logan, 2003; Venkataraman et al., 2005), CO emissions from biofuel

874   burning must be substantial (Lelieveld et al., 2001). This is the case for NE India located

875   upwind of PON and PBL when the NE monsoon prevails during December–March.

876   Nevertheless, the relatively low $\Delta CH_4/\Delta CO$ derived from biomass/biofuel burning could be

877   increased by CH_4 emissions from livestock with similarly distributed sources (EDGAR v4.2).

878   Emissions of both trace gases from livestock and biomass/biofuel burning in the Indian

879   subcontinent compiled by EDGAR v4.2 also indicate a CH_4 to CO ratio of 0.64–0.69 over the

880   period of 2000–2008, close to the atmospheric measurements of $\Delta CH_4/\Delta CO$ at PON and PBL

881   during JFM (Fig. 14h and l).

882

883   **3.2.2 $\Delta CH_4/\Delta CO_2$**

884   The $\Delta CH_4/\Delta CO_2$ ratios are strongly influenced by the high variability of CO_2 and the

885   interpretation is complex. Unlike the positive correlation between CH_4 and CO consistently

886   observed at all three stations, the relationships between CH_4 and CO_2 residuals exhibit

887   scattered and differences in the residual slopes for different stations and seasons (Fig. 15). At

888   HLE, no significant correlations are found during AMJ, JAS, and OND (Fig. 15a–c), because

889   CH_4 and CO_2 have distinct biogenic and/or photochemical sources and sinks over the

890   northern mid-latitudes. During JFM when biogenic CO_2 fluxes and anthropogenic emissions

891   are positive to the atmosphere, there is a significant and positive relationship between CH_4

892   and CO_2, with a $\Delta CH_4/\Delta CO_2$ ratio of 45.6±1846.8 ppb ppm^{-1} (r=0.37, p=0.03; Fig. 15d). This

893   value is close to the ratio of CH_4 and CO_2 anthropogenic emissions over North Africa (39.1–

894   46.2 mmol mol^{-1}), Central Asia (44.4–49.5 mmol mol^{-1}) and to a lesser degree the Middle

895   East (25.8–28.4 mmol mol^{-1}) during the period of 2000–2010 (EDGAR v4.2), corresponding

896   to the back-trajectories reaching HLE (Fig. 1a). It should be noted that this estimate of

897     $\Delta CH_4/\Delta CO_2$ is subject to large uncertainty according to the standard deviation calculated

898   with 1000 bootstrap replications (Fig. 15d), implying that CH_4 and CO_2 sources of various

899   types and origins influence the HLE records.

900

At PON, in contrast to HLE, positive correlations occur between CH_4 and CO_2 residuals for all seasons except OND, with a $\Delta CH_4/\Delta CO_2$ ratio of 6.7±2.4 ppb ppm^{-1} (r=0.72, p<0.001) in AMJ and 8.5±0.9 ppb ppm^{-1} in JAS (r=0.74, p<0.001), respectively (Fig. 15e and f). The relatively narrow ranges of slopes compared to that for HLE and PBL likely suggest co-located urban and industrial sources in South India upwind of PON during April–September (see back-trajectories in Fig. 1a). Emissions from biofuel burning could be a common source for both CH_4 and CO_2, given the substantial biofuel use in South India (Yevich and Logan, 2003) and the biofuel burning emission ratio of CH_4 and CO_2 derived from previous studies (5–10 mmol mol^{-1}; Andreae and Merlet, 2001). Note that the CARIBIC flask measurements over India south of 20°N indicate a negative correlation between CH_4 and CO_2 at the altitudes of 10-12 km during July–September, 2008 (r=-0.80, p=0.002; Fig. S15a), interpreted as the concurrent strong uptake of CO_2 with enhanced emissions of CH_4 during the SW monsoon. During JFM when the NE monsoon predominates, CH_4 is positively correlated with CO_2 with a $\Delta CH_4/\Delta CO_2$ ratio of 31.9±1635.7 ppb ppm^{-1} (r=0.45, p=0.02; Fig. 15h). Like at HLE, this ratio is subject to large uncertainty due to variability in CH_4 and CO_2 sources. The ratio based on the CARIBIC observations in the upper troposphere (10-12 km) is 23.5±41.4 ppb ppm^{-1} (r=0.67, p=0.004; Fig. S15b). The inconsistency of the $\Delta CH_4/\Delta CO_2$ ratios estimated from the two datasets suggest that the flask measurements at the surface station PON do provide information more specific for constraining estimates of regional CH_4 and CO_2 fluxes.

920

Finally, at PBL, the prominent feature of the CH_4–CO_2 relationship is the significant and negative correlation observed during JAS, with a $\Delta CH_4/\Delta CO_2$ ratio of -14.6±16.4 ppb ppm^{-1} (r=-0.73, p=0.007; Fig. 15j). Since the time series of flask measurements at PBL is relatively short and has large data gaps (Fig. S3), correlations between trace gases could be influenced

925   by abnormal pollution events. For example, excluding the event with CH_4 residuals $> +20$

926   ppb (corresponding to the observation at PBL on 16 September 2009, the point marked with

927   black circle in Fig. 15j) would substantially decrease the strength of negative correlation

928   between CH_4 and CO_2 (r=-0.54, p=0.09). We will investigate the CH_4 enriched event further

929   in Sect. 3.3.

930

931   **3.2.3 $\Delta CO/\Delta CO_2$**

932   As shown in Fig. 16, at HLE, CO is positively correlated with CO_2 during AMJ, with a

933     $\Delta CO/\Delta CO_2$ ratio of 35.8 ± 12.1 ppb ppm^{-1} (r=0.53, p=0.001; Fig. 16a). During JFM, there is

934   no significant relationship between CO and CO_2 (r=0.15, p=0.39; Fig. 16d). However,

935   excluding an abnormal event with $\Delta CO_2 = -1.8$ ppm on 8 January 2007 (the point marked

936   with black circle in Fig. 16d) would give a significant and positive correlation between CO

937   and CO_2, with a $\Delta CO/\Delta CO_2$ ratio of 55.7 ± 259.1 ppb ppm^{-1} (r=0.40, p=0.02; the red solid line

938   in Fig. 16d). This ratio is less than half the emission ratio of CO to CO_2 from forest/grassland

939   biomass burning (Mauzerall et al., 1998; Andreae and Merlet, 2001), but higher than ratios of

940   anthropogenic combustion sources in developed countries that are typically in the range of

941   10–15 ppb ppm^{-1} (e.g., Suntharalingam et al., 2004; Wada et al., 2011; Takegawa et al., 2004).

942   This could be attributed not only to the lower combustion efficiency of fuels in North Africa,

943   the Middle East, and Central Asia where air masses at HLE originate from, but also to

944   additional contribution from biofuel burning with relatively high CO to CO_2 emission ratios

945   (e.g., fuelwood, charcoal, agricultural residuals; Andreae and Merlet, 2001). Besides, the

946   relatively high $\Delta CO/\Delta CO_2$ in JFM compared to AMJ may further indicate a contribution of

947   CO emissions from residential biofuel burning in winter (Wada et al., 2011), especially in

948   developing countries within the footprint area.

949

950   At PON, a positive and significant correlation between CO and CO_2 is found during AMJ,

951   with a $\Delta CO/\Delta CO_2$ ratio of 13.4 ± 76.8 ppb ppm^{-1} (r=0.46, p=0.03; Fig. 16e). This ratio is

952   similar to the ratios determined for air masses influenced by both fossil fuel emissions and

953   biomass/biofuel burning during the same seasons. For example, based on the in-situ

954   measurements in the upper troposphere during the CARIBIC flights between South China

955   and Philippines in April 2007, Lai et al. (2010) reported the $\Delta CO/\Delta CO_2$ ratios of 15.6–29.3

956   ppb ppm^{-1} during pollution events influenced by both biomass/biofuel burning and fossil fuel

957   combustion in Indochinese Peninsula. At PBL, CO is significantly and negatively correlated

958   with CO_2 during JAS (r=-0.68, p=0.01; Fig. 16j). However, we note that the CH_4 abnormal

959   event discussed in Sect. 3.2.2 is enriched in CO as well, and the negative relationship

960   between CO and CO_2 would no longer exist if we removed the event (r=-0.45, p=0.16). The

961   simultaneous enhancement of CO and CH_4 may suggest possible influences of biomass

962   burning episodes, which we will explore in detail in Sect. 3.3. During JFM, no significant

963   relationship is found between CO and CO_2 for PON or PBL (Fig. 16h and l).

964

965   **3.3 Elevated CH_4 and CO events at PBL**

966   In this section, we discuss two elevated CH_4 and CO events at PBL during the SW monsoon

967   season. Significant enhancements of CH_4 and CO were observed on September 16, 2009

968   (July 29, 2011), with residuals from smoothed curves as high as 34.2 (29.2) ppb and 36.2

969   (17.9) ppb for CH_4 and CO, respectively. We further analyzed CH_4 and CO measurements at

970   Bukit Kototabang (BKT – 0.20 °S, 100.32 °E, 845.00 m a.s.l.), Indonesia, located upwind of

971   PBL when the southwest monsoon prevails. The flask measurements at BKT detected

972   enhanced CH_4 and CO with a magnitude of 38.0 and 66.1 ppb on September 8, 2009, about

973   one week before the occurrence of the first CH_4 and CO event at PBL (Fig. 17a). The in-situ

974   measurements at BKT also showed CH_4 and CO enhancements about one week before the

975   second event at PBL, lasting over the period of 17 July–21 July 2011 (Fig. 17b). The

976   coincidence of the two abnormal CH_4 and CO events at PBL and BKT possibly suggests

977   influences of polluted air masses with common sources and origins. Moreover, the fire

978   radiative power (FRP, mWm^{-2}) during the sampling dates implies that the two abnormal CH_4

979   and CO events could be related to fire emissions in Indonesia (GFAS product version 1.0;

980   Kaiser et al. 2012; Fig. S16). Note that the mechanisms we propose for the abnormal CH_4 and

981   CO events and the possible linkage between PBL and BKT during the SW monsoon season

982   are still speculative. Model experiments are needed to further confirm these hypotheses.

983

4 Conclusions

985   In this paper we present the results of flask measurements of CO_2, CH_4, N_2O, SF_6, CO, and

986   H_2 at three stations in India: Hanle (HLE), Pondicherry (PON) and Port-Blair (PBL), over the

987   period of 2007–2011. Of these three stations, HLE is located at a high altitude and regarded

988   as a continental background station in the mid-latitude of the Northern Hemisphere; PON is a

989   tropical surface station located on the southwest coast of India, while PBL is an oceanic

990   station located on the Andaman Islands, of similar latitude to PON. With a total of 188, 185,

991   and 63 flask pair samples collected respectively from HLE, PON and PBL between 2007 and

992   2011 (for PBL between 2009 and 2011), and analyzed at LSCE, the program represents an

993   important logistical and analytical effort to produce a unique dataset of atmospheric trace gas

994   observations over the Indian subcontinent. The observed records will serve as an important

995   source of information to infer regional patterns of trace gas fluxes and atmospheric transport

996   in this under-documented region. Several conclusions and implications are drawn from the

997   first analyses of the datasets.

998

999 The annual gradients of the atmospheric mole fractions observed at PON and PBL, with

1000 respect to HLE as a reference, suggest significant emission sources of CO_2, CH_4, N_2O, CO,

1001 and H_2 over the footprints of those stations. In particular, the annual mean N_2O mole

1002 fractions at PON and PBL are higher than at HLE by 3.1 ± 0.3 and 3.8 ± 1.7 ppb, notably larger

1003 than the typical N_2O gradients observed between stations in Europe or North America,

1004 indicating substantial N_2O emissions. The analyses of the atmospheric mole fractions with

1005 back-trajectories at the three stations further confirmed emission sources from South and NE

1006 India, and SE Asia, all of which are populous with high demand for food and energy, and

1007 thus high emissions from industrial, residential, and/or agricultural sectors. On the other hand,

1008 despite of substantial anthropogenic GHG emissions in India (whether based on national

1009 inventories or atmospheric observations), unlike the USA and EU countries, its SF_6 emissions

1010 are rather weak.

1011

1012 The seasonal cycles for each trace gas reflect not only the seasonal variations of natural

1013 sources/sinks and anthropogenic emissions over the Indian subcontinent, but also the

1014 seasonally varying atmospheric transport, especially the monsoon circulations (including

1015 convection). Strong influences of the monsoon circulations are well depicted by the

1016 contrasting phases of CH_4 seasonal cycles between HLE and PON/PBL. At HLE, the distinct

1017 CH_4 maximum during June-September is likely related to the enhanced biogenic CH_4

1018 emissions from wetlands and rice paddies in summer, combined with deep convection

1019 associated with the SW monsoon that mixes surface emissions into the mid-to-upper

1020 troposphere. By contrast, the CH_4 seasonal cycles at PON and PBL have seasonal minima

1021 during the SW monsoon season, reflecting influences of southern hemispheric air depleted in

1022 CH_4 transported at low altitudes, as well as high rates of OH oxidation. Covariance between

1023   species variations at the synoptic scale further helps identification and attribution of different

1024   sources and sinks, like fossil fuel combustion, biofuel burning and biogenic emissions.

1025   Besides, measurements of δ^{13}C-CO$_2$ have been recently started for HLE, and the 4-D

1026   distributions of CO$_2$ and CH$_4$ have been realistically simulated using a chemical transport

1027   model (LMDz-OR-INCA, Hauglustaine et al., 2004; Folberth et al., 2006) with zoom over

1028   South and East Asia (manuscript in preparation). Both of them may serve as valuable tools to

1029   disentangle and quantify contributions of different sources and meteorology to trace gas

1030   signals.

1031

1032   Apart from the flask measurements of trace gases presented in this study for the three stations,

1033   in-situ continuous measurements of CO$_2$ and CH$_4$ have also been deployed at HLE, PON and

1034   PBL in parallel, which would considerably contribute to the value of the stations through

1035   high-frequency air sampling. While the three stations have the potential to provide useful

1036   constraints on estimates of trace gas fluxes over South and NE India (for example, Swathi et

1037   al. (2013) reported considerable reduction in the uncertainty of inverted CO$_2$ fluxes over

1038   temperate Eurasia by the inclusion of measurements at HLE), the monitoring network

1039   requires further expansion to sample air masses from other parts of the Indian subcontinent.

1040   Recently a few other atmospheric ground stations have been established in western India

1041   (Bhattacharya et al., 2009; Tiwari et al., 2011; Tiwari et al., 2014; Tiwari and Kumar, 2012)

1042   and the Himalayas (Kumar et al., 2010; Ganesan et al., 2013), with their concentration

1043   footprints covering Central India (e.g., the Sinhagad station; Tiwari et al., 2014; Tiwari and

1044   Kumar, 2012), the Indo-Gangetic Plains and a large extent of the Himalayas (e.g., the

1045   Dajeeling station; Ganesan et al., 2013). More efforts are needed to develop a comprehensive

1046   observation network with adequate spatial and temporal coverage in this region.

1047

References

1061

1062 Attri, S. D., and Tyagi, A.: Climate Profile of India: Contribution to the Indian Network of Climate
1063   Change Assessment (NATIONAL COMMUNICATION-II) Minitry of Environment and Forests,
1064   Met Monograph No. Environment Meteorology-01/2010, India Meteorological Department,
1065   Ministry of Earth Sciences, New Delhi, 2010.
1066 Andreae, M. O., and Merlet, P.: Emission of trace gases and aerosols from biomass burning, Global
1067   Biogeochem. Cy., 15, 955-966, 10.1029/2000gb001382, 2001.
1068 Babu, S. S., Chaubey, J. P., Krishna Moorthy, K., Gogoi, M. M., Kompalli, S. K., Sreekanth, V., Bagare, S.
1069   P., Bhatt, B. C., Gaur, V. K., Prabhu, T. P., and Singh, N. S.: High altitude (4520 m amsl)
1070   measurements of black carbon aerosols over western trans-Himalayas: Seasonal
1071   heterogeneity and source apportionment, J. Geophys. Res.-Atmos., 116, D24201,
1072   10.1029/2011jd016722, 2011.
1073 Baker, A. K., Schuck, T. J., Brenninkmeijer, C. A. M., Rauthe-Schöch, A., Slemr, F., van Velthoven, P. F.
1074   J., and Lelieveld, J.: Estimating the contribution of monsoon-related biogenic production to
1075   methane emissions from South Asia using CARIBIC observations, Geophys. Res. Lett., 39,
1076   L10813, 10.1029/2012gl051756, 2012.
1077 Bakwin, P. S., Tans, P. P., Zhao, C., Ussler, W., and Quesnell, E.: Measurements of carbon dioxide on a
1078   very tall tower, Tellus B, 47, 535-549, 10.1034/j.1600-0889.47.issue5.2.x, 1995.
1079 Bakwin, P. S., Tans, P. P., Hurst, D. F., and Zhao, C.: Measurements of carbon dioxide on very tall
1080   towers: results of the NOAA/CMDL program, Tellus B, 50B, 401-415, 1998.
1081 Bange, H. W., Andreae, M. O., Lal, S., Law, C. S., Naqvi, S. W. A., Patra, P. K., Rixen, T., and Upstill-
1082   Goddard, R. C.: Nitrous oxide emissions from the Arabian Sea: A synthesis, Atmos. Chem.
1083   Phys., 1, 61-71, 10.5194/acp-1-61-2001, 2001.
1084 Bhattacharya, S. K., Borole, D. V., Francey, R. J., Allison, C. E., Steele, L. P., Krummel, P. B.,
1085   Langenfelds, R., Masarie, K. A., Tiwari, Y. K., and Patra, P. K.: Trace gases and CO_2 isotope
1086   records from Cabo de Rama, India, Curr. Sci., 97, 1336-1344, 2009.
1087 Bond, S. W., Vollmer, M. K., Steinbacher, M., Henne, S., and Reimann, S.: Atmospheric molecular
1088   hydrogen (H_2): observations at the high-altitude site Jungfraujoch, Switzerland, Tellus B, 63,
1089   64-76, 10.1111/j.1600-0889.2010.00509.x, 2011.
1090 Bousquet, P., Yver, C., Pison, I., Li, Y. S., Fortems, A., Hauglustaine, D., Szopa, S., Rayner, P. J., Novelli,
1091   P., Langenfelds, R., Steele, P., Ramonet, M., Schmidt, M., Foster, P., Morfopoulos, C., and
1092   Ciais, P.: A three-dimensional synthesis inversion of the molecular hydrogen cycle: Sources
1093   and sinks budget and implications for the soil uptake, J. Geophys. Res.-Atmos., 116, D01302,
1094   10.1029/2010jd014599, 2011.
1095 Busenberg, E. and Plummer, L. N.: Dating young groundwater with sulfur hexafluoride: Natural and
1096   anthropogenic sources of sulfur hexafluoride, Water Resour. Res., 36(10), 3011–3030,
1097   doi:10.1029/2000WR900151, 2000.
1098 Chi, X., Winderlich, J., Mayer, J. C., Panov, A. V., Heimann, M., Birmili, W., Heintzenberg, J., Cheng, Y.,
1099   and Andreae, M. O.: Long-term measurements of aerosol and carbon monoxide at the
1100   ZOTTO tall tower to characterize polluted and pristine air in the Siberian taiga, Atmos. Chem.
1101   Phys., 13, 12271-12298, 10.5194/acp-13-12271-2013, 2013.
1102 Dlugokencky, E. J., Myers, R. C., Lang, P. M., Masarie, K. A., Crotwell, A. M., Thoning, K. W., Hall, B. D.,
1103   Elkins, J. W., and Steele, L. P.: Conversion of NOAA atmospheric dry air CH_4 mole fractions to
1104   a gravimetrically prepared standard scale, J. Geophys. Res.-Atmos., 110, D18306,
1105   10.1029/2005jd006035, 2005.
1106 Dlugokencky, E.J., P.M. Lang, A.M. Crotwell, K.A. Masarie, and Crotwell, M. J.: Atmospheric Methane
1107   Dry Air Mole Fractions from the NOAA ESRL Carbon Cycle Cooperative Global Air Sampling
1108   Network, 1983-2013, Version: 2014-06-24, Path:
1109   ftp://aftp.cmdl.noaa.gov/data/trace_gases/ch4/flask/surface/ (last access: 11 December
1110   2014), 2014a.

1111 Dlugokencky, E.J., P.M. Lang, K.A. Masarie, A.M. Crotwell, and Crotwell, M.J.: Atmospheric Carbon
1112   Dioxide Dry Air Mole Fractions from the NOAA ESRL Carbon Cycle Cooperative Global Air
1113   Sampling   Network,   1968-2013,   Version: 2014-06-27,   Path:
1114   ftp://aftp.cmdl.noaa.gov/data/trace_gases/co2/flask/surface/ (last access: 11 December
1115   2014), 2014b.
1116 Draxler, R. R., and Rolph, G. D.: HYSPLIT (HYbrid Single-Particle Lagrangian Integrated Trajectory),
1117   Model access via NOAA ARL READY website http://www.arl.noaa.gov/ready/hysplit4.html
1118   (last access: 9 January 2014), NOAA Air Resources Laboratory, Silver Spring, MD, 2003.
1119 Duncan, B. N., Martin, R. V., Staudt, A. C., Yevich, R., and Logan, J. A.: Interannual and seasonal
1120   variability of biomass burning emissions constrained by satellite observations, , J. Geophys.
1121   Res.-Atmos., 108, 4100, 10.1029/2002jd002378, 2003.
1122 EC-JRC/PBL (European Commission, Joint Research Centre/Netherlands Environmental Assessment
1123   Agency): Emission Database for Global Atmospheric Research (EDGAR), release version 4.2:
1124   available at: http://edgar.jrc.ec.europa.eu (last access: 16 August 2014), 2011
1125 Ehhalt, D. H., and Rohrer, F.: The tropospheric cycle of H_2: a critical review, Tellus B, 61, 500-535,
1126   10.1111/j.1600-0889.2009.00416.x, 2009.
1127 Fang, S.-X., Zhou, L.-X., Masarie, K. A., Xu, L. and Rella, C. W.: Study of atmospheric CH_4 mole
1128   fractions at three WMO/GAW stations in China, J. Geophys. Res.-Atmos., 118(10), 4874–
1129   4886, doi:10.1002/jgrd.50284, 2013.
1130 Fang, S. X., Zhou, L. X., Tans, P. P., Ciais, P., Steinbacher, M., Xu, L., and Luan, T.: In situ measurement
1131   of atmospheric CO_2 at the four WMO/GAW stations in China, Atmos. Chem. Phys., 14, 2541-
1132   2554, 10.5194/acp-14-2541-2014, 2014.
1133 Folberth, G. A., Hauglustaine, D. A., Lathière, J. and Brocheton, F.: Interactive chemistry in the
1134   Laboratoire de Météorologie Dynamique general circulation model: model description and
1135   impact analysis of biogenic hydrocarbons on tropospheric chemistry, Atmos. Chem. Phys.,
1136   6(8), 2273–2319, doi:10.5194/acp-6-2273-2006, 2006.
1137 Gadgil, S.: The Indian Monsoon and its variability, Annu. Rev. Earth Planet Sci., 31, 429-467,
1138   10.1146/annurev.earth.31.100901.141251, 2003.
1139 Gamnitzer, U., Karstens, U., Kromer, B., Neubert, R. E. M., Meijer, H. A. J., Schroeder, H., and Levin, I.:
1140   Carbon monoxide: A quantitative tracer for fossil fuel CO_2?, J. Geophys. Res.-Atmos., 111,
1141   D22302, 10.1029/2005jd006966, 2006.
1142 Ganesan, A. L., Chatterjee, A., Prinn, R. G., Harth, C. M., Salameh, P. K., Manning, A. J., Hall, B. D.,
1143   Mühle, J., Meredith, L. K., Weiss, R. F., O'Doherty, S., and Young, D.: The variability of
1144   methane, nitrous oxide and sulfur hexafluoride in Northeast India, Atmos. Chem. Phys., 13,
1145   10633-10644, 10.5194/acp-13-10633-2013, 2013.
1146 Garg, A., Shukla, P. R., Kapshe, M., and Menon, D.: Indian methane and nitrous oxide emissions and
1147   mitigation flexibility, Atmos. Environ., 38, 1965-1977, http://dx.doi.org/10.1016/
1148   j.atmosenv.2003.12.032, 2004.
1149 Garg, A., Shukla, P. R., and Upadhyay, J.: N_2O emissions of India: an assessment of temporal, regional
1150   and sector trends, Clim. Change, 110, 755-782, 10.1007/s10584-011-0094-9, 2012.
1151 Goswami, B. N.: South Asian Monsoon, in: Intraseasonal variability in the Atmosphere-Ocean Climate
1152   System, edited by: Lau, W. K. M., and Waliser, D. E., Springer & Praxis Publishing, Chichester,
1153   UK, 2005.
1154 Granier, C., Bessagnet, B., Bond, T., D'Angiola, A., Denier van der Gon, H., Frost, G., Heil, A., Kaiser, J.,
1155   Kinne, S., Klimont, Z., Kloster, S., Lamarque, J.-F., Liousse, C., Masui, T., Meleux, F., Mieville,
1156   A., Ohara, T., Raut, J.-C., Riahi, K., Schultz, M., Smith, S., Thompson, A., van Aardenne, J., van
1157   der Werf, G. and van Vuuren, D.: Evolution of anthropogenic and biomass burning emissions
1158   of air pollutants at global and regional scales during the 1980–2010 period, Clim. Change,
1159   109(1-2), 163–190, doi:10.1007/s10584-011-0154-1, 2011.

Grant, A., Witham, C. S., Simmonds, P. G., Manning, A. J., and O'Doherty, S.: A 15 year record of high-frequency, in situ measurements of hydrogen at Mace Head, Ireland, Atmos. Chem. Phys., 10, 1203-1214, 10.5194/acp-10-1203-2010, 2010.

Hall, B. D., Dutton, G. S., and Elkins, J. W.: The NOAA nitrous oxide standard scale for atmospheric observations, J. Geophys. Res.-Atmos., 112, D09305, 10.1029/2006jd007954, 2007.

Harris, J. M., Dlugokencky, E. J., Oltmans, S. J., Tans, P. P., Conway, T. J., Novelli, P. C., Thoning, K. W., and Kahl, J. D. W.: An interpretation of trace gas correlations during Barrow, Alaska, winter dark periods, 1986–1997, J. Geophys. Res.-Atmos., 105, 17267-17278, 10.1029/2000jd900167, 2000.

Harriss, R. C., Sachse, G. W., Collins, J. E., Wade, L., Bartlett, K. B., Talbot, R. W., Browell, E. V., Barrie, L. A., Hill, G. F., and Burney, L. G.: Carbon monoxide and methane over Canada: July–August 1990, J. Geophys. Res.-Atmos., 99, 1659-1669, 10.1029/93jd01906, 1994.

Haszpra, L., Barcza, Z., Hidy, D., Szilágyi, I., Dlugokencky, E., and Tans, P.: Trends and temporal variations of major greenhouse gases at a rural site in Central Europe, Atmos. Environ., 42, 8707-8716, http://dx.doi.org/10.1016/j.atmosenv.2008.09.012, 2008.

Hauglustaine, D. A., and Ehhalt, D. H.: A three-dimensional model of molecular hydrogen in the troposphere, J. Geophys. Res.- Atmos., 107, 4330, 10.1029/2001jd001156, 2002.

Hauglustaine, D. A., Hourdin, F., Jourdain, L., Filiberti, M. A., Walters, S., Lamarque, J. F., and Holland, E. A.: Interactive chemistry in the Laboratoire de Météorologie Dynamique general circulation model: Description and background tropospheric chemistry evaluation, J. Geophys. Res.-Atmos., 109, D04314, 10.1029/2003jd003957, 2004.

Huang, J., Golombek, A., Prinn, R., Weiss, R., Fraser, P., Simmonds, P., Dlugokencky, E. J., Hall, B., Elkins, J., Steele, P., Langenfelds, R., Krummel, P., Dutton, G. and Porter, L.: Estimation of regional emissions of nitrous oxide from 1997 to 2005 using multinetwork measurements, a chemical transport model, and an inverse method, J. Geophys. Res.-Atmos., 113(D17), D17313, doi:10.1029/2007JD009381, 2008.

IPCC: Climate Change 2013: The Physical Science Basis. Contribution of Working Group I to the Fifth Assessment Report of the Intergovernmental Panel on Climate Change, Cambridge University Press, Cambridge, 2013.

IPCC: Climate Change 2014: Impacts, Adaptation, and Vulnerability. Part A: Global and Sectoral Aspects. Contribution of Working Group II to the Fifth Assessment Report of the Intergovernmental Panel on Climate Change [Field, C.B., V.R. Barros, D.J. Dokken, K.J. Mach, M.D. Mastrandrea, T.E. Bilir, M. Chatterjee, K.L. Ebi, Y.O. Estrada, R.C. Genova, B. Girma, E.S. Kissel, A.N. Levy, S. MacCracken, P.R. Mastrandrea, and L.L. White (eds.)], Cambridge University Press, Cambridge, United Kingdom and New York, NY, USA, 2014a.

IPCC: Climate Change 2014: Impacts, Adaptation, and Vulnerability. Part B: Regional Aspects. Contribution of Working Group II to the Fifth Assessment Report of the Intergovernmental Panel on Climate Change [Barros, V.R., C.B. Field, D.J. Dokken, M.D. Mastrandrea, K.J. Mach, T.E. Bilir, M. Chatterjee, K.L. Ebi, Y.O. Estrada, R.C. Genova, B. Girma, E.S. Kissel, A.N. Levy, S. MacCracken, P.R. Mastrandrea, and L.L. White (eds.)], Cambridge University Press, Cambridge, United Kingdom and New York, NY, USA, 2014b.

Jiang, J. H., Livesey, N. J., Su, H., Neary, L., McConnell, J. C., and Richards, N. A. D.: Connecting surface emissions, convective uplifting, and long-range transport of carbon monoxide in the upper troposphere: New observations from the Aura Microwave Limb Sounder, Geophys. Res. Lett., 34, L18812, 10.1029/2007gl030638, 2007a.

Jiang, X., Ku, W. L., Shia, R.-L., Li, Q., Elkins, J. W., Prinn, R. G., and Yung, Y. L.: Seasonal cycle of N_2O: Analysis of data, Global Biogeochemical Cycles, 21, GB1006, 10.1029/2006gb002691, 2007b.

Jordan, A., and Steinberg, B.: Calibration of atmospheric hydrogen measurements, Atmos. Meas. Tech., 4, 509-521, 10.5194/amt-4-509-2011, 2011.

Kaiser, J. W., Heil, A., Andreae, M. O., Benedetti, A., Chubarova, N., Jones, L., Morcrette, J. J., Razinger, M., Schultz, M. G., Suttie, M., and van der Werf, G. R.: Biomass burning emissions

estimated with a global fire assimilation system based on observed fire radiative power, Biogeosciences, 9, 527-554, 10.5194/bg-9-527-2012, 2012.

Kaplan, J. O., Folberth, G. and Hauglustaine, D. A.: Role of methane and biogenic volatile organic compound sources in late glacial and Holocene fluctuations of atmospheric methane concentrations, Global Biogeochem. Cycles, 20(2), GB2016, doi:10.1029/2005GB002590, 2006.

Kasischke, E. S., Hyer, E. J., Novelli, P. C., Bruhwiler, L. P., French, N. H. F., Sukhinin, A. I., Hewson, J. H., and Stocks, B. J.: Influences of boreal fire emissions on Northern Hemisphere atmospheric carbon and carbon monoxide, Global Biogeochem. Cy., 19, GB1012, 10.1029/2004gb002300, 2005.

King, A. W., Andres, R. J., Davis, K. J., Hafer, M., Hayes, D. J., Huntzinger, D. N., de Jong, B., Kurz, W. A., McGuire, A. D., Vargas, R., Wei, Y., West, T. O. and Woodall, C. W.: North America's net terrestrial CO_2 exchange with the atmosphere 1990–2009, Biogeosciences, 12(2), 399–414, doi:10.5194/bg-12-399-2015, 2015.

Konovalov, I. B., Berezin, E. V., Ciais, P., Broquet, G., Beekmann, M., Hadji-Lazaro, J., Clerbaux, C., Andreae, M. O., Kaiser, J. W., and Schulze, E. D.: Constraining CO_2 emissions from open biomass burning by satellite observations of co-emitted species: a method and its application to wildfires in Siberia, Atmos. Chem. Phys., 14, 10383-10410, 10.5194/acp-14-10383-2014, 2014.

Kumar, R., Naja, M., Venkataramani, S., and Wild, O.: Variations in surface ozone at Nainital: A high-altitude site in the central Himalayas, J. Geophys. Res.-Atmos., 115, D16302, 10.1029/2009jd013715, 2010.

Kurokawa, J., Ohara, T., Morikawa, T., Hanayama, S., Janssens-Maenhout, G., Fukui, T., Kawashima, K., and Akimoto, H.: Emissions of air pollutants and greenhouse gases over Asian regions during 2000–2008: Regional Emission inventory in ASia (REAS) version 2, Atmos. Chem. Phys., 13, 11019-11058, 10.5194/acp-13-11019-2013, 2013.

Lai, S. C., Baker, A. K., Schuck, T. J., van Velthoven, P., Oram, D. E., Zahn, A., Hermann, M., Weigelt, A., Slemr, F., Brenninkmeijer, C. A. M., and Ziereis, H.: Pollution events observed during CARIBIC flights in the upper troposphere between South China and the Philippines, Atmos. Chem. Phys., 10, 1649-1660, 10.5194/acp-10-1649-2010, 2010.

Lal, S., Chandra, N., Venkataramani, S.: A study of CO_2 and related trace gases using a laser based technique at an urban site in western India. Submitted to Curr. Sci., 2015.

Langenfelds, R. L., Francey, R. J., Pak, B. C., Steele, L. P., Lloyd, J., Trudinger, C. M., and Allison, C. E.: Interannual growth rate variations of atmospheric CO_2 and its $\delta^{13}C$, H_2, CH_4, and CO between 1992 and 1999 linked to biomass burning, Global Biogeochem. Cy., 16, 1048, 10.1029/2001gb001466, 2002.

Lawrence, M. G., and Lelieveld, J.: Atmospheric pollutant outflow from southern Asia: a review, Atmos. Chem. Phys., 10, 11017-11096, 10.5194/acp-10-11017-2010, 2010.

Lelieveld, J., Crutzen, P. J., Ramanathan, V., Andreae, M. O., Brenninkmeijer, C. A. M., Campos, T., Cass, G. R., Dickerson, R. R., Fischer, H., de Gouw, J. A., Hansel, A., Jefferson, A., Kley, D., de Laat, A. T. J., Lal, S., Lawrence, M. G., Lobert, J. M., Mayol-Bracero, O. L., Mitra, A. P., Novakov, T., Oltmans, S. J., Prather, K. A., Reiner, T., Rodhe, H., Scheeren, H. A., Sikka, D., and Williams, J.: The Indian Ocean Experiment: Widespread Air Pollution from South and Southeast Asia, Science, 291, 1031-1036, 2001.

Le Quéré, C., Moriarty, R., Andrew, R. M., Peters, G. P., Ciais, P., Friedlingstein, P., Jones, S. D., Sitch, S., Tans, P., Arneth, A., Boden, T. A., Bopp, L., Bozec, Y., Canadell, J. G., Chevallier, F., Cosca, C. E., Harris, I., Hoppema, M., Houghton, R. A., House, J. I., Jain, A. K., Johannessen, T., Kato, E., Keeling, R. F., Kitidis, V., Klein Goldewijk, K., Koven, C., Landa, C. S., Landschützer, P., Lenton, A., Lima, I. D., Marland, G. H., Mathis, J. T., Metzl, N., Nojiri, Y., Olsen, A., Ono, T., Peters, W., Pfeil, B., Poulter, B., Raupach, M. R., Regnier, P., Rödenbeck, C., Saito, S., Sailsbury, J. E., Schuster, U., Schwinger, J., Séférian, R., Segschneider, J., Steinhoff, T., Stocker, B. D., Sutton,

1262   A. J., Takahashi, T., Tilbrook, B., van der Werf, G. R., Viovy, N., Wang, Y.-P., Wanninkhof, R.,
1263   Wiltshire, A., and Zeng, N.: Global Carbon Budget 2014. Earth Syst. Sci. Data Discuss.,
1264   doi:10.5194/essdd-7-521-2014, 2014

1265 Levin, I., Ciais, P., Langenfelds, R., Schmidt, M., Ramonet, M., Sidorov, K., Tchebakova, N., Gloor, M.,
1266   Heimann, M., Schulze, E. D., Vygodskaya, N. N., Shibistova, O., and Lloyd, J.: Three years of
1267   trace gas observations over the EuroSiberian domain derived from aircraft sampling — a
1268   concerted action, Tellus B, 54, 696-712, 10.1034/j.1600-0889.2002.01352.x, 2002.

1269 Li, Q., Jiang, J. H., Wu, D. L., Read, W. G., Livesey, N. J., Waters, J. W., Zhang, Y., Wang, B., Filipiak, M.
1270   J., Davis, C. P., Turquety, S., Wu, S., Park, R. J., Yantosca, R. M., and Jacob, D. J.: Convective
1271   outflow of South Asian pollution: A global CTM simulation compared with EOS MLS
1272   observations, Geophys. Res. Lett., 32, L14826, 10.1029/2005gl022762, 2005.

1273 Liao, T., Camp, C. D., and Yung, Y. L.: The seasonal cycle of N_2O, Geophys. Res. Lett., 31, L17108,
1274   10.1029/2004gl020345, 2004.

1275 Logan, J. A., Prather, M. J., Wofsy, S. C., and McElroy, M. B.: Tropospheric chemistry: A global
1276   perspective, J. Geophys. Res.-Oceans, 86, 7210-7254, 10.1029/JC086iC08p07210, 1981.

1277 Lopez, M.: Estimation des émissions de gaz à effet de serre à différentes échelles en France à l'aide
1278   d'observations de haute précision, Ph.D, Université Paris-Sud, 2012.

1279 Lopez, M., Schmidt, M., Ramonet, M., Bonne, J.-L., Colomb, A., Kazan, V., Laj, P., and Pichon, J.-M.: A
1280   gas chromatograph system for semi-continuous greenhouse gas measurements at Puy de
1281   Dôme station, Centeral France, Atmos. Meas. Tech. Discuss., 8(3), 3121–3170,
1282   doi:10.5194/amtd-8-3121-2015, 2015.

1283 Luyssaert, S., Abril, G., Andres, R., Bastviken, D., Bellassen, V., Bergamaschi, P., Bousquet, P.,
1284   Chevallier, F., Ciais, P., Corazza, M., Dechow, R., Erb, K.-H., Etiope, G., Fortems-Cheiney, A.,
1285   Grassi, G., Hartmann, J., Jung, M., Lathière, J., Lohila, A., Mayorga, E., Moosdorf, N., Njakou,
1286   D. S., Otto, J., Papale, D., Peters, W., Peylin, P., Raymond, P., Rödenbeck, C., Saarnio, S.,
1287   Schulze, E.-D., Szopa, S., Thompson, R., Verkerk, P. J., Vuichard, N., Wang, R., Wattenbach, M.
1288   and Zaehle, S.: The European land and inland water CO_2, CO, CH_4 and N_2O balance between
1289   2001 and 2005, Biogesciences, 9(8), 3357–3380, doi:10.5194/bg-9-3357-2012, 2012.

1290 Machida, T., Matsueda, H., Sawa, Y., Nakagawa, Y., Hirotani, K., Kondo, N., Goto, K., Nakazawa, T.,
1291   Ishikawa, K., and Ogawa, T.: Worldwide Measurements of Atmospheric CO_2 and Other Trace
1292   Gas Species Using Commercial Airlines, J. Atmos. Ocean. Tech., 25, 1744-1754,
1293   10.1175/2008jtecha1082.1, 2008.

1294 Maiss, M., Steele, L. P., Francey, R. J., Fraser, P. J., Langenfelds, R. L., Trivett, N. B. A., and Levin, I.:
1295   Sulfur hexafluoride—A powerful new atmospheric tracer, Atmos. Environ., 30, 1621-1629,
1296   http://dx.doi.org/10.1016/1352-2310(95)00425-4, 1996.

1297 Matthews, E., Fung, I. and Lerner, J.: Methane emission from rice cultivation: Geographic and
1298   seasonal distribution of cultivated areas and emissions, Global Biogeochem. Cycles, 5(1), 3–
1299   24, doi:10.1029/90GB02311, 1991.

1300 Mauzerall, D. L., Logan, J. A., Jacob, D. J., Anderson, B. E., Blake, D. R., Bradshaw, J. D., Heikes, B.,
1301   Sachse, G. W., Singh, H., and Talbot, B.: Photochemistry in biomass burning plumes and
1302   implications for tropospheric ozone over the tropical South Atlantic, J. Geophys. Res.-Atmos.,
1303   103, 8401-8423, 10.1029/97jd02612, 1998.

1304 Messager, C.: Estimation des flux de gaz à effet de serre à l'échelle régionale à partir de mesures
1305   atmosphériques, Université Paris 7 - Denis Diderot, 2007.

1306 Ministry of Environment and Forests, Government of India (MoEF): India Second National
1307   Communication to the United Nations Framework Convention on Climate Change, New Delhi.
1308   [online] Available from: http://unfccc.int/resource/docs/natc/indnc2.pdf, 2012.

1309 Minschwaner, K., Salawitch, R. J., and McElroy, M. B.: Absorption of solar radiation by O_2:
1310   Implications for O_3 and lifetimes of N_2O, $CFCl_3$, and CF_2Cl_2, J. Geophys. Res.-Atmos., 98,
1311   10543-10561, 10.1029/93jd00223, 1993.

1312 Montzka, S. A., Dlugokencky, E. J., and Butler, J. H.: Non-CO_2 greenhouse gases and climate change,
1313   Nature, 476, 43-50, 2011.
1314 Moorthy, K. K., Sreekanth, V., Chaubey, J. P., Gogoi, M. M., Babu, S. S., Kompalli, S. K., Bagare, S. P.,
1315   Bhatt, B. C., Gaur, V. K., Prabhu, T. P., Singh, N. S.: Fine and ultrafine particles at near-free
1316   tropospheric environment over the high-altitude station Hanle in the Trans-Himalaya: New
1317   particle formation and size distribution, J. Geophys. Res.-Atmos., 116, D20212, doi: 10.1029/
1318   2011JD016343, 2011
1319 Morgan, C. G., Allen, M., Liang, M. C., Shia, R. L., Blake, G. A., and Yung, Y. L.: Isotopic fractionation of
1320   nitrous oxide in the stratosphere: Comparison between model and observations, J. Geophys.
1321   Res.-Atmos., 109, D04305, 10.1029/2003jd003402, 2004.
1322 Morris, R. A., Miller, T. M., Viggiano, A. A., Paulson, J. F., Solomon, S., and Reid, G.: Effects of electron
1323   and ion reactions on atmospheric lifetimes of fully fluorinated compounds, J. Geophys. Res.-
1324   Atmos., 100, 1287-1294, 10.1029/94jd02399, 1995.
1325 Mühle, J., Brenninkmeijer, C. A. M., Rhee, T. S., Slemr, F., Oram, D. E., Penkett, S. A., and Zahn, A.:
1326   Biomass burning and fossil fuel signatures in the upper troposphere observed during a
1327   CARIBIC flight from Namibia to Germany, Geophys. Res. Lett., 29, 1910,
1328   10.1029/2002gl015764, 2002.
1329 Niwa, Y., Machida, T., Sawa, Y., Matsueda, H., Schuck, T. J., Brenninkmeijer, C. A. M., Imasu, R., and
1330   Satoh, M.: Imposing strong constraints on tropical terrestrial CO_2 fluxes using passenger
1331   aircraft based measurements, J. Geophys. Res.-Atmos., 117, D11303, 10.1029/
1332   2012jd017474, 2012.
1333 Niwa, Y., Tsuboi, K., Matsueda, H., Sawa, Y., Machida, T., Nakamura, M., Kawasato, T., Saito, K.,
1334   Takatsuji, S., Tsuji, K., Nishi, H., Dehara, K., Baba, Y., Kuboike, D., Iwatsubo, S., Ohmori, H.,
1335   and Hanamiya, Y.: Seasonal Variations of CO_2, CH_4, N_2O and CO in the Mid-Troposphere over
1336   the Western North Pacific Observed Using a C-130H Cargo Aircraft, J. Meteor. Soc. Japan. Ser.
1337   II, 92, 55-70, 10.2151/jmsj.2014-104, 2014.
1338 Novelli, P. C., Steele, L. P., and Tans, P. P.: Mixing ratios of carbon monoxide in the troposphere, J.
1339   Geophys. Res.-Atmos., 97, 20731-20750, 10.1029/92jd02010, 1992.
1340 Novelli, P. C., Masarie, K. A., and Lang, P. M.: Distributions and recent changes of carbon monoxide
1341   in the lower troposphere, J. Geophys. Res.-Atmos., 103, 19015-19033, 10.1029/98jd01366,
1342   1998.
1343 Novelli, P. C., Lang, P. M., Masarie, K. A., Hurst, D. F., Myers, R., and Elkins, J. W.: Molecular hydrogen
1344   in the troposphere: Global distribution and budget, J. Geophys. Res.-Atmos., 104, 30427-
1345   30444, 10.1029/1999jd900788, 1999.
1346 Novelli, P. C., Lang, P. M., and Masarie, K. A.: Atmospheric Hydrogen Dry Air Mole Fractions from the
1347   NOAA ESRL Carbon Cycle Cooperative Global Air Sampling Network, 1988-2009, Version:
1348   2014-08-27, Path: ftp://aftp.cmdl.noaa.gov/data/trace_gases/h2/flask/surface/ (last access:
1349   11 December 2014), 2014a.
1350 Novelli, P.C. and Masarie, K.A.: Atmospheric Carbon Monoxide Dry Air Mole Fractions from the
1351   NOAA ESRL Carbon Cycle Cooperative Global Air Sampling Network, 1988-2013, Version:
1352   2014-07-02, Path: ftp://aftp.cmdl.noaa.gov/data/trace_gases/co/flask/surface/ (last access:
1353   11 December 2014), 2014b.
1354 Olivier, J. G. J., Van Aardenne, J. A., Dentener, F., Ganzeveld, L. and Peters, J. A. H. W.: Recent trends
1355   in global greenhouse gas emissions: regional trends and spatial distribution of key sources, in
1356   Non-CO_2 Greenhouse Gases (NCGG-4), edited by A. Van Amstel, pp. 325–330, Millpress,
1357   Rotterdam, The Netherlands., 2005.
1358 Paris, J. D., Ciais, P., NÉDÉLec, P., Ramonet, M., Belan, B. D., Arshinov, M. Y., Golitsyn, G. S., Granberg,
1359   I., Stohl, A., Cayez, G., Athier, G., Boumard, F., and Cousin, J. M.: The YAK-AEROSIB
1360   transcontinental aircraft campaigns: new insights on the transport of CO_2, CO and O_3 across
1361   Siberia, Tellus B, 60, 551-568, 10.1111/j.1600-0889.2008.00369.x, 2008.

Park, M., Randel, W. J., Gettelman, A., Massie, S. T., and Jiang, J. H.: Transport above the Asian summer monsoon anticyclone inferred from Aura Microwave Limb Sounder tracers, J. Geophys. Res.-Atmos., 112, D16309, 10.1029/2006jd008294, 2007.

Pathak, H., Bhatia, A., Jain, N., and Aggarwal, P. K.: Greenhouse Gas Emission and Mitigation in Indian Agriculture - A Review, in: ING Bulletins on Regional Assessment of Reactive Nitrogen, Bulletin No. 19, edited by: Singh, B., SCON-ING, New Delhi, i-iv & 1-34, 2010.

Patra, P., Takigawa, M., Ishijima, K., Choi, B.-C., Cunnold, D., J. Dlugokencky, E., Fraser, P., J. Gomez-Pelaez, A., Goo, T.-Y., Kim, J.-S., Krummel, P., Langenfelds, R., Meinhardt, F., Mukai, H., O'Doherty, S., Prinn, R. G., Simmonds, P., Steele, P., Tohjima, Y., Tsuboi, K., Uhse, K., Weiss, R., Worthy, D., and Nakazawa, T.: Growth Rate, Seasonal, Synoptic, Diurnal Variations and Budget of Methane in the Lower Atmosphere, J. Meteor. Soc. Japan. Ser. II, 87, 635-663, 2009.

Patra, P. K., Lal, S., Venkataramani, S., de Sousa, S. N., Sarma, V. V. S. S., and Sardesai, S.: Seasonal and spatial variability in N_2O distribution in the Arabian Sea, Deep Sea Res. Part I: Oceanogr Res. Pap., 46, 529-543, http://dx.doi.org/10.1016/S0967-0637(98)00071-5, 1999.

Patra, P. K., Houweling, S., Krol, M., Bousquet, P., Belikov, D., Bergmann, D., Bian, H., Cameron-Smith, P., Chipperfield, M. P., Corbin, K., Fortems-Cheiney, A., Fraser, A., Gloor, E., Hess, P., Ito, A., Kawa, S. R., Law, R. M., Loh, Z., Maksyutov, S., Meng, L., Palmer, P. I., Prinn, R. G., Rigby, M., Saito, R., and Wilson, C.: TransCom model simulations of CH_4 and related species: linking transport, surface flux and chemical loss with CH_4 variability in the troposphere and lower stratosphere, Atmos. Chem. Phys., 11, 12813-12837, 10.5194/acp-11-12813-2011, 2011a.

Patra, P. K., Niwa, Y., Schuck, T. J., Brenninkmeijer, C. A. M., Machida, T., Matsueda, H., and Sawa, Y.: Carbon balance of South Asia constrained by passenger aircraft CO_2 measurements, Atmos. Chem. Phys., 11, 4163-4175, 10.5194/acp-11-4163-2011, 2011b.

Patra, P. K., Canadell, J. G., Houghton, R. A., Piao, S. L., Oh, N. H., Ciais, P., Manjunath, K. R., Chhabra, A., Wang, T., Bhattacharya, T., Bousquet, P., Hartman, J., Ito, A., Mayorga, E., Niwa, Y., Raymond, P. A., Sarma, V. V. S. S., and Lasco, R.: The carbon budget of South Asia, Biogeosciences, 10, 513-527, 10.5194/bg-10-513-2013, 2013.

Peylin, P., Law, R. M., Gurney, K. R., Chevallier, F., Jacobson, A. R., Maki, T., Niwa, Y., Patra, P. K., Peters, W., Rayner, P. J., Rödenbeck, C., and Zhang, X.: Global atmospheric carbon budget: results from an ensemble of atmospheric CO_2 inversions, Biogeosciences Discuss., 10, 5301-5360, 10.5194/bgd-10-5301-2013, 2013.

Pison, I., Bousquet, P., Chevallier, F., Szopa, S., and Hauglustaine, D.: Multi-species inversion of CH_4, CO and H_2 emissions from surface measurements, Atmos. Chem. Phys., 9, 5281-5297, 10.5194/acp-9-5281-2009, 2009.

Press, W.H., Teukolsky, S.A., Vetterling, W.T., Flannery, B.P., 2007. Straight-Line Data with Errors in Both Coordinates, in: Numerical Recipes: The Art of Scientific Computing. Cambridge University Press, New York, pp. 785–788.

Price, H., Jaeglé, L., Rice, A., Quay, P., Novelli, P. C., and Gammon, R.: Global budget of molecular hydrogen and its deuterium content: Constraints from ground station, cruise, and aircraft observations, J. Geophys. Res.-Atmos., 112, D22108, 10.1029/2006jd008152, 2007.

R Core Team: R: A language and environment for statistical computing. R Foundation for Statistical computing, Vienna, Austria. Available from: http://www.r-project.org/, 2014.

Ramonet, M., Ciais, P., Nepomniachii, I., Sidorov, K., Neubert, R. E. M., Langendörfer, U., Picard, D., Kazan, V., Biraud, S., Gusti, M., Kolle, O., Schulze, E. D., and Lloyd, J.: Three years of aircraft-based trace gas measurements over the Fyodorovskoye southern taiga forest, 300 km north-west of Moscow, Tellus B, 54, 713-734, 10.1034/j.1600-0889.2002.01358.x, 2002.

Ravishankara, A. R., Daniel, J. S. and Portmann, R. W.: Nitrous oxide (N_2O): The dominant ozone-depleting substance emitted in the 21st century, Science, 326(5949), 123–125, doi:10.1126/science.1176985, 2009.

Ravishankara, A. R., Solomon, S., Turnipseed, A. A., and Warren, R. F.: Atmospheric lifetimes of long-lived halogenated species, Science, 259, 194-199, 1993.

Rayner, P. J., Law, R. M., Allison, C. E., Francey, R. J., Trudinger, C. M., and Pickett-Heaps, C.: Interannual variability of the global carbon cycle (1992–2005) inferred by inversion of atmospheric CO_2 and $\delta^{13}CO_2$ measurements, Global Biogeochem. Cy., 22, GB3008, 10.1029/2007gb003068, 2008.

Rivier, L., Ciais, P., Hauglustaine, D. A., Bakwin, P., Bousquet, P., Peylin, P., and Klonecki, A.: Evaluation of SF_6, C_2Cl_4, and CO to approximate fossil fuel CO_2 in the Northern Hemisphere using a chemistry transport model, J. Geophys. Res.-Atmos., 111, D16311, 10.1029/2005jd006725, 2006.

Saikawa, E., Prinn, R. G., Dlugokencky, E., Ishijima, K., Dutton, G. S., Hall, B. D., Langenfelds, R., Tohjima, Y., Machida, T., Manizza, M., Rigby, M., O'Doherty, S., Patra, P. K., Harth, C. M., Weiss, R. F., Krummel, P. B., van der Schoot, M., Fraser, P. J., Steele, L. P., Aoki, S., Nakazawa, T., and Elkins, J. W.: Global and regional emissions estimates for N_2O, Atmos. Chem. Phys., 14, 4617-4641, 10.5194/acp-14-4617-2014, 2014.

Sawa, Y., Matsueda, H., Makino, Y., Inoue, H. Y., Murayama, S., Hirota, M., Tsutsumi, Y., Zaizen, Y., Ikegami, M., and Okada, K.: Aircraft Observation of CO_2, CO, O_3 and H_2 over the North Pacific during the PACE-7 Campaign, Tellus B, 56, 2-20, 10.1111/j.1600-0889.2004.00088.x, 2004.

Schuck, T. J., Brenninkmeijer, C. A. M., Baker, A. K., Slemr, F., von Velthoven, P. F. J., and Zahn, A.: Greenhouse gas relationships in the Indian summer monsoon plume measured by the CARIBIC passenger aircraft, Atmos. Chem. Phys., 10, 3965-3984, 10.5194/acp-10-3965-2010, 2010.

Schuck, T. J., Ishijima, K., Patra, P. K., Baker, A. K., Machida, T., Matsueda, H., Sawa, Y., Umezawa, T., Brenninkmeijer, C. A. M., and Lelieveld, J.: Distribution of methane in the tropical upper troposphere measured by CARIBIC and CONTRAIL aircraft, J. Geophys. Res.-Atmos., 117, D19304, 10.1029/2012jd018199, 2012.

Seinfeld, J. H. and Pandis, S. N.: Atmospheric Chemistry and Physics: From Air Pollution to Climate Change, John Wiley and Sons, Hoboken, New Jersey, USA., 2006.

Sivakumar, I., and Anitha, M.: Education and girl children in Puducherry region: Problems and perspective, Int. J. Soc. Sci. Interdiscipl. Res., 1, 175-184, 2012.

Streets, D. G., Bond, T. C., Carmichael, G. R., Fernandes, S. D., Fu, Q., He, D., Klimont, Z., Nelson, S. M., Tsai, N. Y., Wang, M. Q., Woo, J. H., and Yarber, K. F.: An inventory of gaseous and primary aerosol emissions in Asia in the year 2000, J. Geophys. Res.-Atmos., 108, 8809, 10.1029/2002jd003093, 2003a.

Streets, D. G., Yarber, K. F., Woo, J. H., and Carmichael, G. R.: Biomass burning in Asia: Annual and seasonal estimates and atmospheric emissions, Global Biogeochem. Cy., 17, 1099, 10.1029/2003gb002040, 2003b.

Suntharalingam, P., Jacob, D. J., Palmer, P. I., Logan, J. A., Yantosca, R. M., Xiao, Y., Evans, M. J., Streets, D. G., Vay, S. L., and Sachse, G. W.: Improved quantification of Chinese carbon fluxes using CO_2/CO correlations in Asian outflow, J. Geophys. Res.-Atmos., 109, D18S18, 10.1029/2003jd004362, 2004.

Swathi, P. S., Indira, N. K., Rayner, P. J., Ramonet, M., Jagadheesha, D., Bhatt, B. C., Gaur, V. K.: Robust inversion of carbon dioxide fluxes over temperate Eurasia in 2006-2008, Curr. Sci., 105, 201-208, 2013.

Takegawa, N., Kondo, Y., Koike, M., Chen, G., Machida, T., Watai, T., Blake, D. R., Streets, D. G., Woo, J. H., Carmichael, G. R., Kita, K., Miyazaki, Y., Shirai, T., Liley, J. B., and Ogawa, T.: Removal of NO_x and NO_y in Asian outflow plumes: Aircraft measurements over the western Pacific in January 2002, J. Geophys. Res.-Atmos., 109, D23S04, 10.1029/2004jd004866, 2004.

Teetor, P., 2011. Performing Simple Orthogonal Regression, in: Loukides, M. (Ed.), R Cookbook. O'Reilly Media, Sebastopol, pp. 340–341.

Thompson, R. L., Chevallier, F., Crotwell, A. M., Dutton, G., Langenfelds, R. L., Prinn, R. G., Weiss, R. F., Tohjima, Y., Nakazawa, T., Krummel, P. B., Steele, L. P., Fraser, P., O'Doherty, S., Ishijima, K., and Aoki, S.: Nitrous oxide emissions 1999 to 2009 from a global atmospheric inversion, Atmos. Chem. Phys., 14, 1801-1817, 10.5194/acp-14-1801-2014, 2014a.

Thompson, R. L., Ishijima, K., Saikawa, E., Corazza, M., Karstens, U., Patra, P. K., Bergamaschi, P., Chevallier, F., Dlugokencky, E., Prinn, R. G., Weiss, R. F., O'Doherty, S., Fraser, P. J., Steele, L. P., Krummel, P. B., Vermeulen, A., Tohjima, Y., Jordan, A., Haszpra, L., Steinbacher, M., Van der Laan, S., Aalto, T., Meinhardt, F., Popa, M. E., Moncrieff, J., and Bousquet, P.: TransCom N_2O model inter-comparison – Part 2: Atmospheric inversion estimates of N_2O emissions, Atmos. Chem. Phys., 14, 6177-6194, 10.5194/acp-14-6177-2014, 2014b.

Thompson, R. L., Patra, P. K., Ishijima, K., Saikawa, E., Corazza, M., Karstens, U., Wilson, C., Bergamaschi, P., Dlugokencky, E., Sweeney, C., Prinn, R. G., Weiss, R. F., O'Doherty, S., Fraser, P. J., Steele, L. P., Krummel, P. B., Saunois, M., Chipperfield, M., and Bousquet, P.: TransCom N_2O model inter-comparison – Part 1: Assessing the influence of transport and surface fluxes on tropospheric N_2O variability, Atmos. Chem. Phys., 14, 4349-4368, 10.5194/acp-14-4349-2014, 2014c.

Thoning, K. W., Tans, P. P., and Komhyr, W. D.: Atmospheric carbon dioxide at Mauna Loa Observatory: 2. Analysis of the NOAA GMCC data, 1974–1985, J. Geophys. Res.-Atmos., 94, 8549-8565, 10.1029/JD094iD06p08549, 1989.

Tiwari, Y. K., Patra, P. K., Chevallier, F., Francey, R. J., Krummel, P. B., Allison, C. E., Revadekar, J. V., Chakraborty, S., Langenfelds, R. L., Bhattacharya, S. K., Borole, D. V., Kumar, K. R., and Steele, L. P.: Carbon dioxide observations at Cape Rama, India for the period 1993-2002: implications for constraining Indian emissions, Curr. Sci., 101, 1562-1568, 2011.

Tiwari, Y. K., and Kumar, K. R.: GHG observation programs in India, in: Asian GAW greenhouse gases Newsletter, Volume No. 3, Korea Meteorological Administration, Chungnam, South Korea, 2012.

Tiwari, Y. K., Revadekar, J. V., and Ravi Kumar, K.: Variations in atmospheric Carbon Dioxide and its association with rainfall and vegetation over India, Atmos. Environ., 68, 45-51, http://dx.doi.org/10.1016/j.atmosenv.2012.11.040, 2013.

Tiwari, Y. K., Vellore, R. K., Ravi Kumar, K., van der Schoot, M., and Cho, C.-H.: Influence of monsoons on atmospheric CO_2 spatial variability and ground-based monitoring over India, Sci. Total Environ., 490, 570-578, http://dx.doi.org/10.1016/j.scitotenv.2014.05.045, 2014.

Tohjima, Y., Maksyutov, S., Machida, T., and Inoue, G.: Airborne measurements of atmospheric methane over oil fields in western Siberia, Geophys. Res. Lett., 23, 1621-1624, 10.1029/96gl01027, 1996.

Turnbull, J. C., Miller, J. B., Lehman, S. J., Tans, P. P., Sparks, R. J., and Southon, J.: Comparison of 14CO2, CO, and SF6 as tracers for recently added fossil fuel CO2 in the atmosphere and implications for biological CO_2 exchange, Geophys. Res. Lett., 33, L01817, 10.1029/2005gl024213, 2006.

Valsala, V., Tiwari, Y. K., Pillai, P., Roxy, M., Maksyutov, S., and Murtugudde, R.: Intraseasonal variability of terrestrial biospheric CO_2 fluxes over India during summer monsoons, J. Geophys. Res.-Biogeo., 118, 752-769, 10.1002/jgrg.20037, 2013.

van der Werf, G. R., Randerson, J. T., Giglio, L., Collatz, G. J., Kasibhatla, P. S., and Arellano Jr, A. F.: Interannual variability in global biomass burning emissions from 1997 to 2004, Atmos. Chem. Phys., 6, 3423-3441, 10.5194/acp-6-3423-2006, 2006.

van der Werf, G. R., Randerson, J. T., Giglio, L., Collatz, G. J., Mu, M., Kasibhatla, P. S., Morton, D. C., DeFries, R. S., Jin, Y., and van Leeuwen, T. T.: Global fire emissions and the contribution of deforestation, savanna, forest, agricultural, and peat fires (1997–2009), Atmos. Chem. Phys., 10, 11707-11735, 10.5194/acp-10-11707-2010, 2010.

1511   Venkataraman, C., Habib, G., Eiguren-Fernandez, A., Miguel, A. H., and Friedlander, S. K.: Residential
1512   Biofuels in South Asia: Carbonaceous Aerosol Emissions and Climate Impacts, Science, 307,
1513   1454-1456, 2005.
1514   Volk, C. M., Elkins, J. W., Fahey, D. W., Dutton, G. S., Gilligan, J. M., Loewenstein, M., Podolske, J. R.,
1515   Chan, K. R., and Gunson, M. R.: Evaluation of source gas lifetimes from stratospheric
1516   observations, J. Geophys. Res.-Atmos., 102, 25543-25564, 10.1029/97jd02215, 1997.
1517   Wada, A., Matsueda, H., Sawa, Y., Tsuboi, K., and Okubo, S.: Seasonal variation of enhancement
1518   ratios of trace gases observed over 10 years in the western North Pacific, Atmos. Environ., 45,
1519   2129-2137, http://dx.doi.org/10.1016/j.atmosenv.2011.01.043, 2011.
1520   Wang, R., Tao, S., Ciais, P., Shen, H. Z., Huang, Y., Chen, H., Shen, G. F., Wang, B., Li, W., Zhang, Y. Y.,
1521   Lu, Y., Zhu, D., Chen, Y. C., Liu, X. P., Wang, W. T., Wang, X. L., Liu, W. X., Li, B. G., and Piao, S.
1522   L.: High-resolution mapping of combustion processes and implications for CO_2 emissions,
1523   Atmos. Chem. Phys., 13, 5189-5203, 10.5194/acp-13-5189-2013, 2013.
1524   Xiao, Y., Jacob, D. J., Wang, J. S., Logan, J. A., Palmer, P. I., Suntharalingam, P., Yantosca, R. M.,
1525   Sachse, G. W., Blake, D. R., and Streets, D. G.: Constraints on Asian and European sources of
1526   methane from CH_4-C_2H_6-CO correlations in Asian outflow, J. Geophys. Res.-Atmos., 109,
1527   D15S16, 10.1029/2003jd004475, 2004.
1528   Xiong, X., Houweling, S., Wei, J., Maddy, E., Sun, F., and Barnet, C.: Methane plume over south Asia
1529   during the monsoon season: satellite observation and model simulation, Atmos. Chem. Phys.,
1530   9, 783-794, 10.5194/acp-9-783-2009, 2009.
1531   Yan, X., Cai, Z., Ohara, T., and Akimoto, H.: Methane emission from rice fields in mainland China:
1532   Amount and seasonal and spatial distribution, J. Geophys. Res.-Atmos., 108, 4505,
1533   10.1029/2002jd003182, 2003.
1534   Yashiro, H., Sudo, K., Yonemura, S., and Takigawa, M.: The impact of soil uptake on the global
1535   distribution of molecular hydrogen: chemical transport model simulation, Atmos. Chem.
1536   Phys., 11, 6701-6719, 10.5194/acp-11-6701-2011, 2011.
1537   Yevich, R., and Logan, J. A.: An assessment of biofuel use and burning of agricultural waste in the
1538   developing world, Global Biogeochem. Cy., 17, 1095, 10.1029/2002gb001952, 2003.
1539   Yver, C., Schmidt, M., Bousquet, P., Zahorowski, W., and Ramonet, M.: Estimation of the molecular
1540   hydrogen soil uptake and traffic emissions at a suburban site near Paris through hydrogen,
1541   carbon monoxide, and radon-222 semicontinuous measurements, J. Geophys. Res.-Atmos.,
1542   114, D18304, 10.1029/2009jd012122, 2009.
1543   Yver, C.: Estimation des sources et puits du dihydrogène troposphérique - développements
1544   instrumentaux, mesures atmosphériques et assimilation variationnelle, Ph.D dissertation,
1545   Université de Versailles - Saint Quentin, 2010.
1546   Yver, C. E., Pison, I. C., Fortems-Cheiney, A., Schmidt, M., Chevallier, F., Ramonet, M., Jordan, A.,
1547   Søvde, O. A., Engel, A., Fisher, R. E., Lowry, D., Nisbet, E. G., Levin, I., Hammer, S., Necki, J.,
1548   Bartyzel, J., Reimann, S., Vollmer, M. K., Steinbacher, M., Aalto, T., Maione, M., Arduini, J.,
1549   O'Doherty, S., Grant, A., Sturges, W. T., Forster, G. L., Lunder, C. R., Privalov, V., Paramonova,
1550   N., Werner, A., and Bousquet, P.: A new estimation of the recent tropospheric molecular
1551   hydrogen budget using atmospheric observations and variational inversion, Atmos. Chem.
1552   Phys., 11, 3375-3392, 10.5194/acp-11-3375-2011, 2011.
1553   Zhang, F., Zhou, L. X., Novelli, P. C., Worthy, D. E. J., Zellweger, C., Klausen, J., Ernst, M., Steinbacher,
1554   M., Cai, Y. X., Xu, L., Fang, S. X., and Yao, B.: Evaluation of in situ measurements of
1555   atmospheric carbon monoxide at Mount Waliguan, China, Atmos. Chem. Phys., 11, 5195-
1556   5206, 10.5194/acp-11-5195-2011, 2011.
1557   Zhang, H. F., Chen, B. Z., Machida, T., Matsueda, H., Sawa, Y., Fukuyama, Y., Langenfelds, R., van der
1558   Schoot, M., Xu, G., Yan, J. W., Cheng, M. L., Zhou, L. X., Tans, P., and Peters, W.: Estimating
1559   Asian terrestrial carbon fluxes from CONTRAIL aircraft and surface CO_2 observations for the
1560   period 2006-2010, Atmos. Chem. Phys., 14, 5807-5824, 10.5194/acp-14-5807-2014, 2014.

1561   Zhang, X. I. A., Nakazawa, T., Ishizawa, M., Aoki, S., Nakaoka, S.-I., Sugawara, S., Maksyutov, S., Saeki,
1562   T., and Hayasaka, T.: Temporal variations of atmospheric carbon dioxide in the southernmost
1563   part of Japan, Tellus B, 59, 654-663, 10.1111/j.1600-0889.2007.00288.x, 2007.
1564   Zhao, C. L., and Tans, P. P.: Estimating uncertainty of the WMO mole fraction scale for carbon
1565   dioxide in air, J. Geophys. Res.-Atmos., 111, D08S09, 10.1029/2005jd006003, 2006.
1566

Table

1568   **Table 1** Annual mean values, trend, and average peak-to-peak amplitudes of trace gases at

1569   HLE, PON, PBL and the two additional NOAA/ESRL stations – KZM and WLG. For each

1570   species at each station, the annual mean values and average peak-to-peak amplitude are

1571   calculated from the smoothed curve and mean seasonal cycle, respectively. The residual

1572   standard deviation (RSD) around the smoothed curve and the Julian days corresponding to

1573   the maximum (D_{max}) and minimum (D_{min}) of the mean seasonal cycle are given as well.

1574   Uncertainty of each estimate is calculated from 1 s.d. of 1000 bootstrap replicates.

	HLE	PON	PBL	KZM	WLG
CO_2 (ppm)					
Annual mean 2007	382.3±0.3	386.6±0.9	–	382.7±0.2	384.2±0.2
Annual mean 2008	384.6±0.5	388.1±0.9	–	385.7±0.2	386.0±0.2
Annual mean 2009	387.2±0.2	389.0±0.6	–	–	387.4±0.2
Annual mean 2010	389.4±0.1	391.3±1.5	387.6±0.7	–	390.1±0.2
Annual mean 2011	391.4±0.3	–	390.2±0.6	–	392.2±0.2
Trend (yr^{-1})	2.1±0.0	1.7±0.1	–	–	2.0±0.0
(Trend at MLO: 2.0±0.0)					
RSD	0.7	4.0	1.5	1.5	1.4
Amplitude	8.2±0.4	7.6±1.4	11.1±1.3	13.8±0.5	11.1±0.4
D_{max}	122.0±2.9	111.0±13.4	97.0±26.0	75.0±2.6	100.0±1.5
D_{min}	261.0±3.0	327.0±54.3	242.0±7.7	205.0±2.1	222.0±1.6
CH_4 (ppb)					
Annual mean 2007	1814.8±2.9	1859.2±6.7	–	1842.6±2.4	1841.0±1.8
Annual mean 2008	1833.1±5.4	1856.1±10.4	–	1856.6±2.3	1845.6±1.5
Annual mean 2009	1830.2±1.7	1865.7±5.1	–	–	1851.8±1.9
Annual mean 2010	1830.5±2.1	1876.9±9.1	1867.5±15.4	–	1857.6±1.4
Annual mean 2011	1849.5±5.2	–	1852.0±7.6	–	1859.9±1.2
Trend (yr^{-1})	4.9±0.0	9.4±0.1	–	–	5.3±0.0
(Trend at MLO: 6.2±0.0)					
RSD	9.1	34.4	22.4	14.6	12.3
Amplitude	28.9±4.2	124.1±10.2	143.9±12.4	22.7±4.7	17.5±2.2
D_{max}	219.0±4.6	337.0±6.1	345.0±87.6	236.0±43.2	222.0±6.2
D_{min}	97.0±58.9	189.0±10.7	193.0±13.5	338.0±39.0	340.0±96.6
N_2O (ppb)					
Annual mean 2007	322.2±0.1	324.8±0.3	–		
Annual mean 2008	322.9±0.1	326.3±0.3	–		
Annual mean 2009	323.5±0.1	326.7±0.3	–		
Annual mean 2010	324.0±0.1	327.1±0.5	329.0±0.5		
Annual mean 2011	325.2±0.1	–	327.9±0.3		

|					
Trend (yr^{-1})	0.8±0.0	0.8±0.1	–		
(Trend at MLO: 1.0±0.0)					
RSD	0.3	1.4	1.1		
Amplitude	0.6±0.1	1.2±0.5	2.2±0.6		
D$_{max}$	227.0±11.8	262.0±83.2	313.0±42.6		
D$_{min}$	115.0±16.4	141.0±48.2	65.0±33.4		
SF$_6$ (ppt)					
Annual mean 2007	6.26±0.03	6.19±0.01	–		
Annual mean 2008	6.54±0.03	6.49±0.02	–		
Annual mean 2009	6.79±0.01	6.77±0.01	–		
Annual mean 2010	7.17±0.01	7.08±0.02	7.10±0.07		
Annual mean 2011	7.38±0.01	–	7.45±0.03		
Trend (yr^{-1})	0.29±0.05	0.31±0.05	–		
(Trend at MLO: 0.29±0.03)					
RSD	0.07	0.05	0.12		
Amplitude	0.15±0.03	0.24±0.02	0.48±0.07		
D$_{max}$	320.0±8.3	327.0±12.1	342.0±59.9		
D$_{min}$	211.0±65.1	204.0±3.3	210.0±18.1		
CO (ppb)					
Annual mean 2007	104.7±1.4	200.5±7.8	–	121.7±1.7	141.0±4.3
Annual mean 2008	103.1±2.1	175.3±13.1	–	123.7±1.7	129.0±2.9
Annual mean 2009	98.9±1.9	174.3±4.8	–	–	131.9±3.7
Annual mean 2010	99.0±1.2	185.1±8.7	157.6±20.4	–	130.2±3.9
Annual mean 2011	99.4±2.2	–	145.9±9.9	–	124.0±2.3
Trend (yr^{-1})	-2.2±0.0	0.4±0.1	–	–	-1.9±0.0
(Trend at MLO: -1.6±0.0)					
RSD	6.5	32.0	30.8	11.8	22.5
Amplitude	28.4±2.3	78.2±11.6	144.1±16.0	37.1±4.4	38.6±5.1
D$_{max}$	79.0±11.4	4.0±160.2	12.0±117.9	72.0±5.0	94.0±38.2
D$_{min}$	297.0±5.3	238.0±46.1	213.0±23.0	318.0±6.1	331.0±6.2
H$_2$ (ppb)					
Annual mean 2007	539.6±2.1	574.5±2.4	–	502.4±2.0	500.9±1.5
Annual mean 2008	533.2±3.2	558.2±5.3	–	–	–
Annual mean 2009	533.3±1.6	562.4±1.6	–	–	–
Annual mean 2010	533.5±1.8	563.9±2.3	558.6±2.4	–	–
Annual mean 2011	536.9±1.5	–	555.4±1.6	–	–
Trend (yr^{-1})	-0.5±0.0	-1.3±0.1	–	–	–
RSD	6.6	8.4	7.0	13.3	9.5
Amplitude	15.8±2.2	21.6±3.4	21.3±5.0	16.7±4.0	22.8±3.0
D$_{max}$	120.0±8.7	96.0±9.6	99.0±8.8	120.0±34.2	51.0±13.4
D$_{min}$	266.0±39.6	219.0±10.3	353.0±87.8	341.0±78.3	298.0±6.5

Figures

1577 **Figure 1 (a)** Five-day back-trajectories calculated for all sampling dates over the period
1578 2007–2011 at Hanle (HLE), Pondicherry (PON), and Port Blair (PBL) during April–June
1579 (AMJ), July–September (JAS), October–December (OND) and January–March (JFM),
1580 respectively. Back-trajectories are colored by the elevation of air masses at hourly time step.
1581 **(b)** Map of terrain over the zoomed box in **(a)**, showing locations of HLE, PON and PBL.
1582 The digital elevation data are obtained from NASA Shuttle Radar Topographic Mission
1583 (SRTM) product at 1km resolution (http://srtm.csi.cgiar.org)

1584
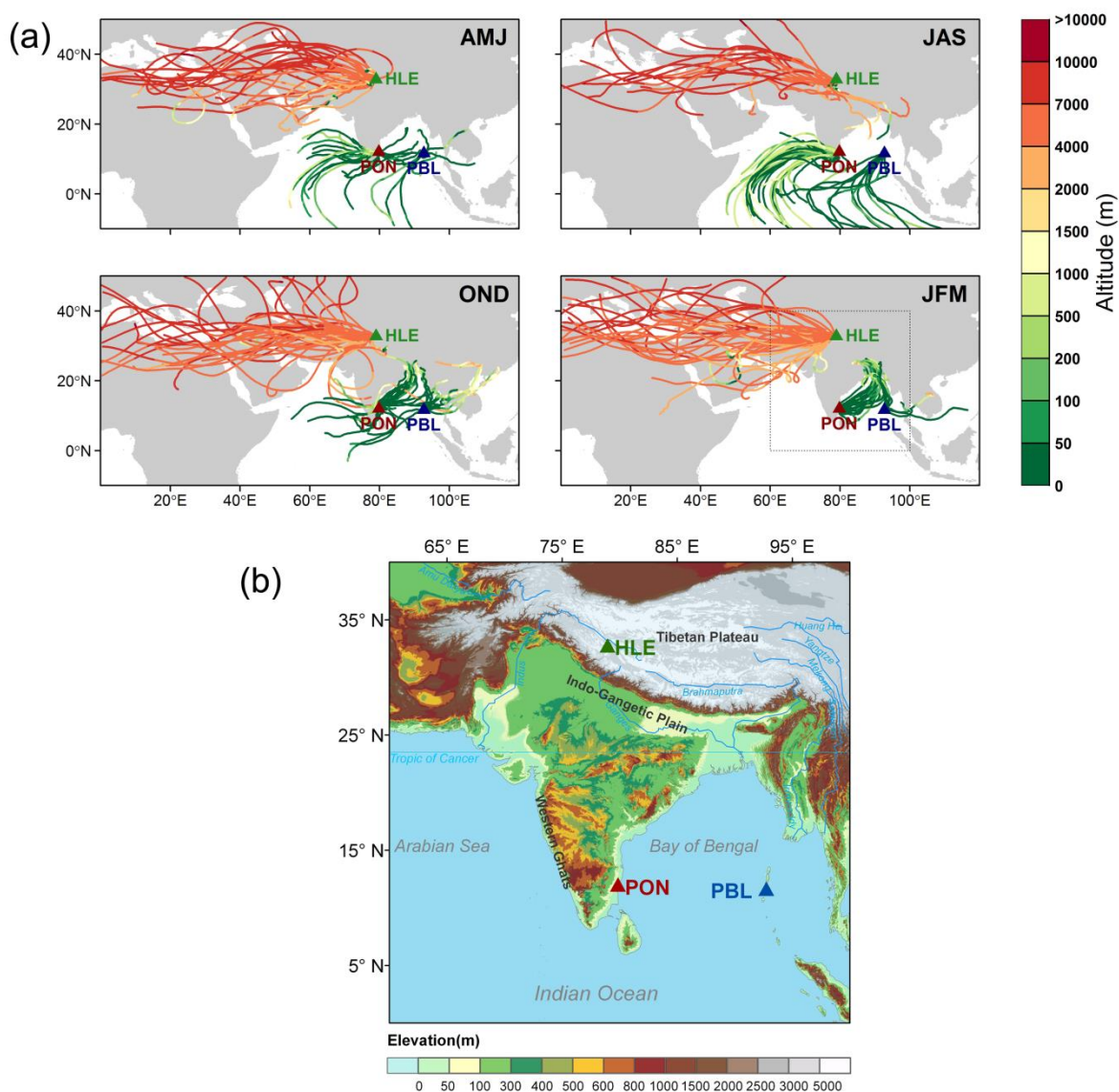
1585   **Figure 2** Time series of CO_2 flask measurements at **(a)** HLE and PON, **(b)** HLE and PBL, **(c)**

1586   HLE and KZM, and **(d)** HLE and WLG. The open circles denote flask data used to fit the

1587   smoothed curves, while the crosses denote discarded flask data lying outside 3 times the

1588   residual standard deviations from the smoothed curve fits. For each station, the smoothed

1589   curve is fitted using Thoning's method (Thoning et al., 1989) after removing outliers.


1590
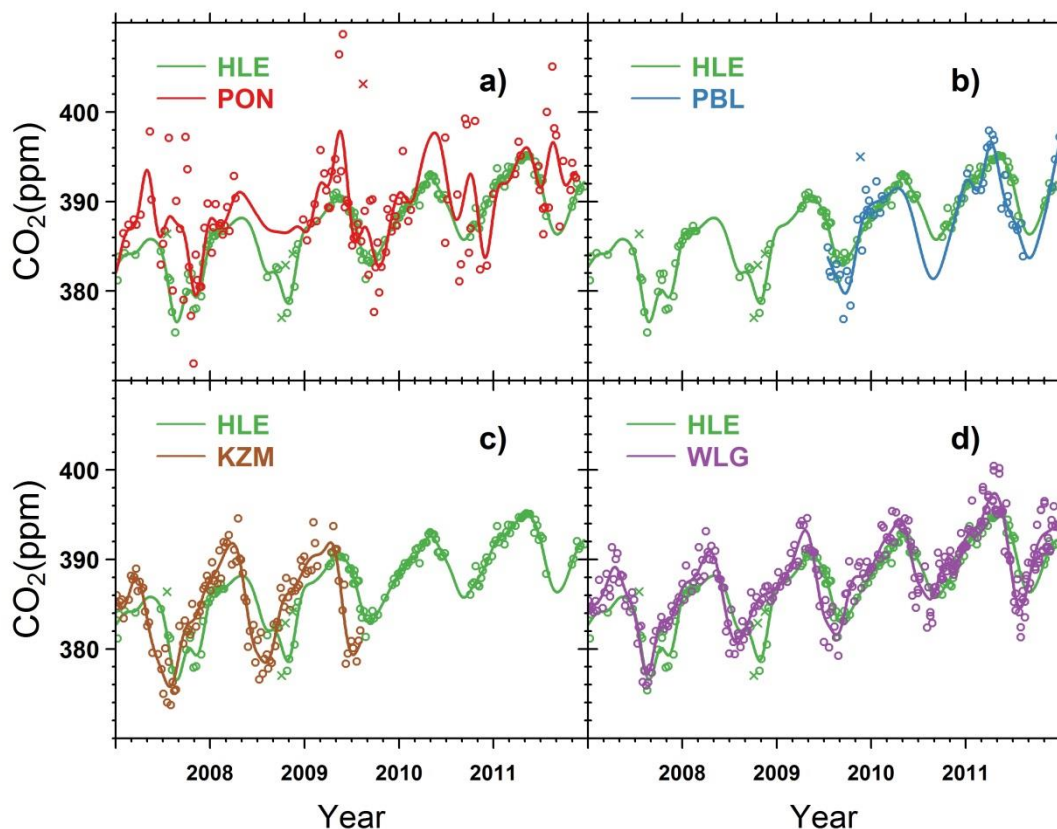
Figure 3 (a) The mean CO_2 seasonal cycle at HLE, in comparison with the mean seasonal

1592 cycles derived from the in-situ CO_2 measurements over New Delhi at different altitude bands

1593 (3–4 km, 4–5 km, and 5–6 km) by the CONTRAIL project (2006–2010). **(b)** The mean CO_2

1594 seasonal cycles at HLE, KZM and WLG. **(c)** The mean CO_2 seasonal cycles at HLE, PON

1595 and PBL. For each station, the mean seasonal cycle is derived from the harmonics of the

1596 smoothed fitting curve in Fig. 2. Shaded area indicates the uncertainty of the mean seasonal

1597 cycle calculated from 1 s.d. of 1000 bootstrap replicates. For the CONTRAIL datasets, CO_2

1598 measurements over New Delhi were first averaged by altitude bands. A fitting procedure was

1599 then applied to the aggregated CO_2 measurements to generate the mean season cycle for

1600 different altitude bands.
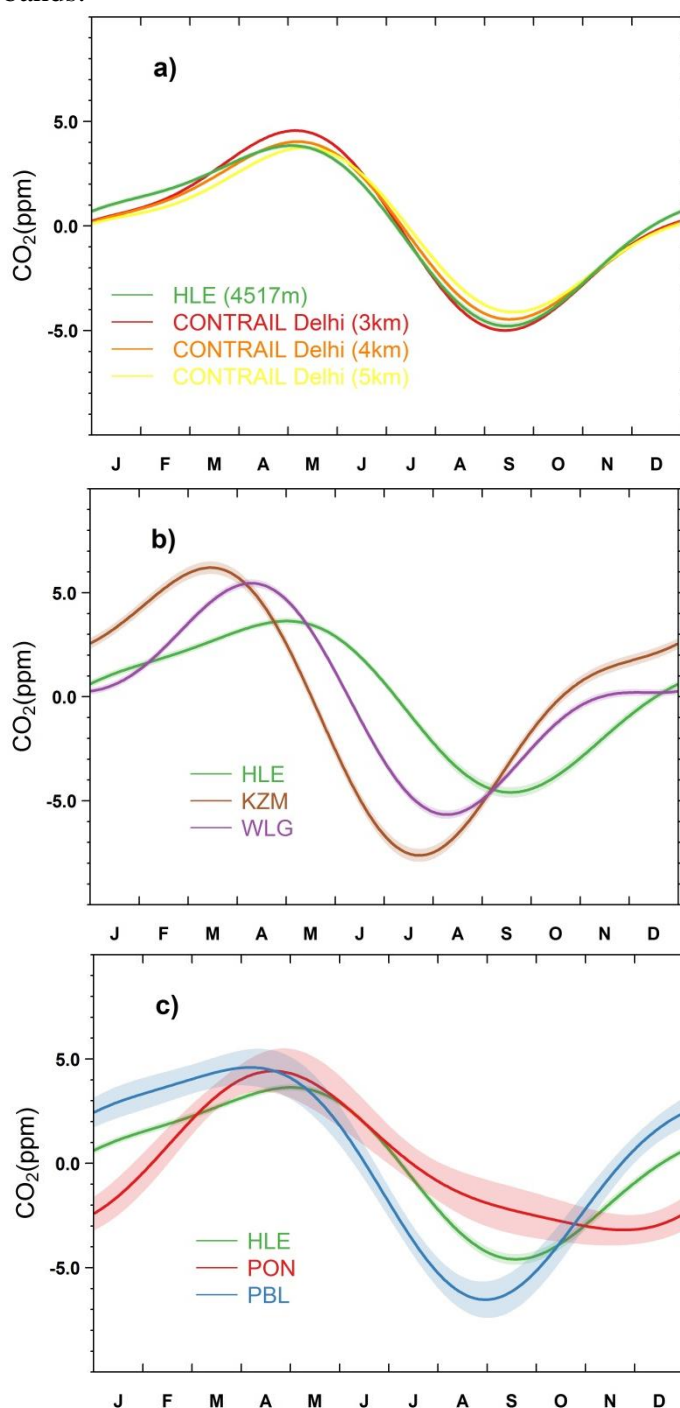
1601   **Figure 4** Time series of CH$_4$ flask measurements at **(a)** HLE and PON, **(b)** HLE and PBL, **(c)**

1602   HLE and KZM, and **(d)** HLE and WLG. The open circles denote flask data used to fit the

1603   smoothed curves, while the crosses denote discarded flask data lying outside 3 times the

1604   residual standard deviations from the smoothed curve fits. For each station, the smoothed

1605   curve is fitted using Thoning's method (Thoning et al., 1989) after removing outliers.
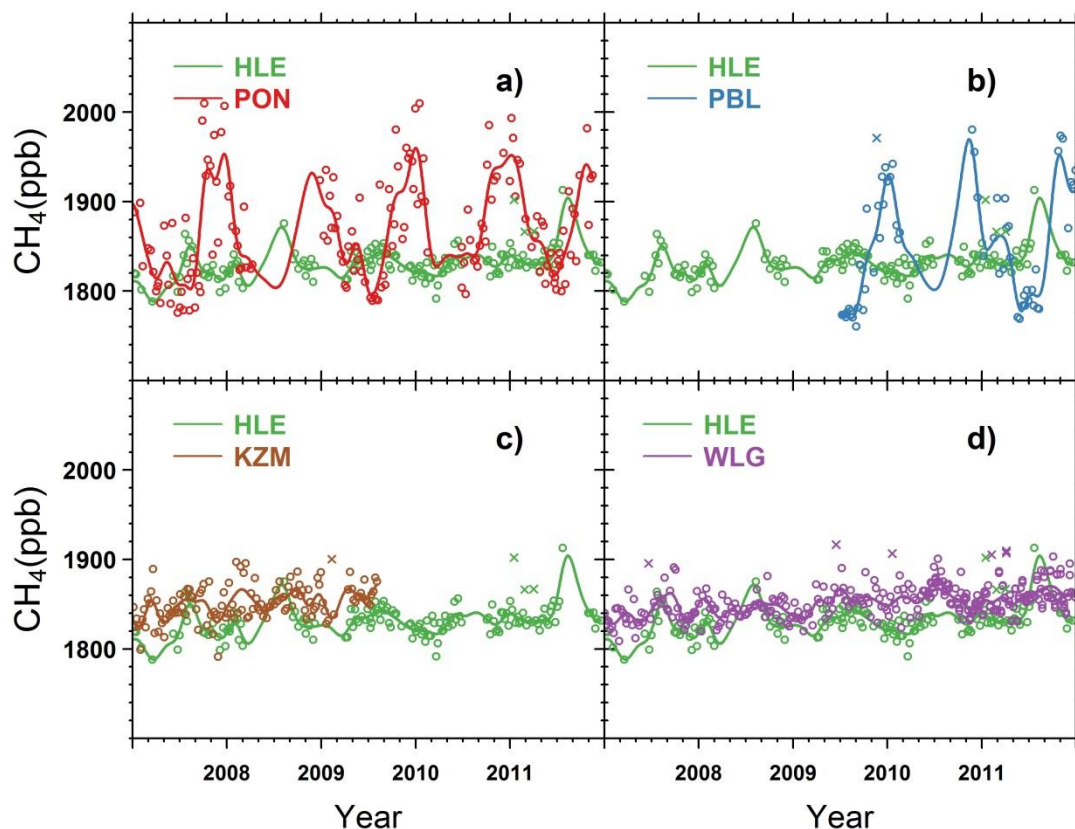
1606
1607

1608   **Figure 5 (a)** The mean CH_4 seasonal cycles observed at HLE, KZM and WLG. The mean

1609 CH_4 seasonal cycle derived from aircraft flask measurements by the CARIBIC project is also

1610   presented. The CARIBIC flask measurements in the upper troposphere (200-300 hPa) during

1611   2005–2012 are averaged over the Indian subcontinent (10°N-35°N, 60°E-100°E) by month to

1612   generate the mean seasonal cycle. The error bars indicate 1 standard deviation of CH_4 flask

1613   measurements within the month. **(b)** The seasonal variations of CH_4 emissions from rice

1614   paddies and wetlands over the Indian subcontinent. The CH_4 emissions from rice paddies are

1615   extracted from a global emission map for the year 2010 (EDGAR v4.2), imposed by the

1616   seasonal variation on the basis of Matthews et al. (1991). The CH_4 emissions from wetlands

1617   are extracted from outputs of a global vegetation model (BIOME4-TG, Kaplan et al., 2006).

1618   The seasonal variation of deep convection over the Indian subcontinent is also presented,

1619   indicated by convective precipitation obtained from an LMDz simulation nudged with

1620   ECMWF reanalysis (Hauglustaine et al., 2004). The CH_4 emissions and convective

1621   precipitation are averaged over the domain 10–35 °N, 70°–90°E to give a regional mean

1622   estimate. **(c)** The mean CH_4 seasonal cycles observed at HLE, PON and PBL. For each

1623   station, the mean seasonal cycle is derived from the harmonics of the smoothed fitting curve

1624   in Fig. 4. Shaded area indicates the uncertainty of the mean seasonal cycle calculated from 1

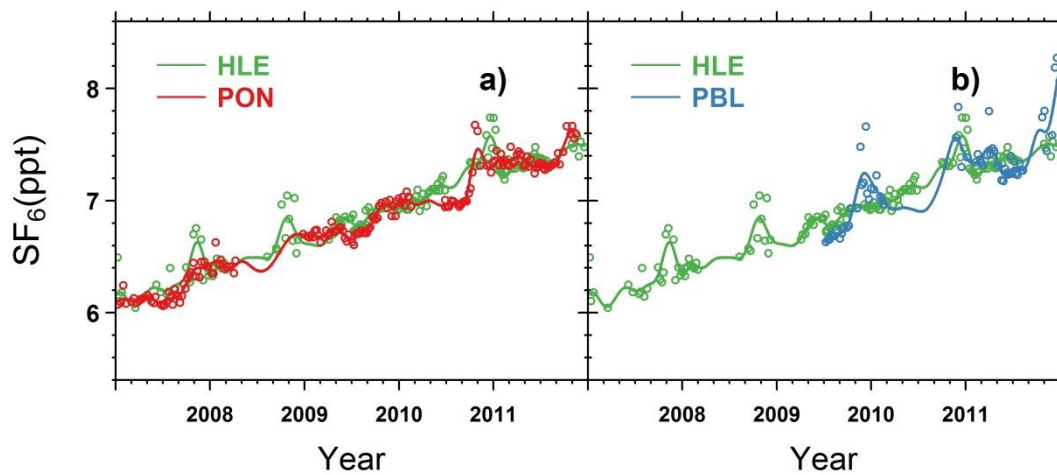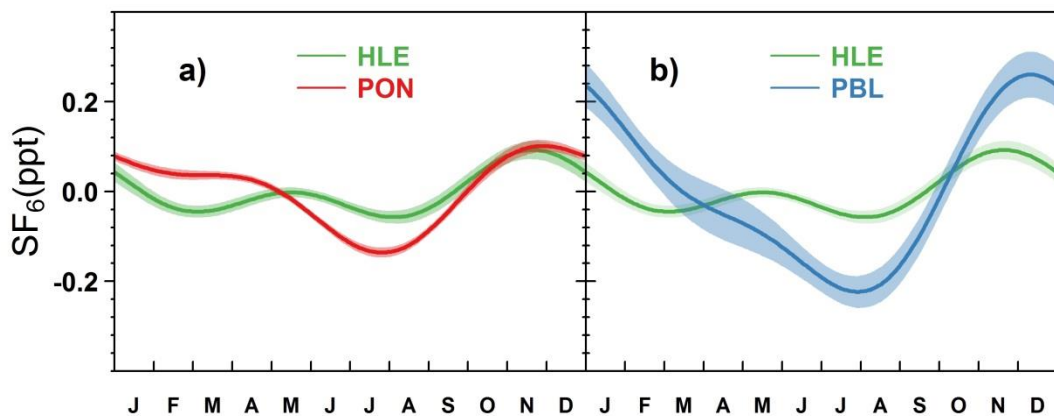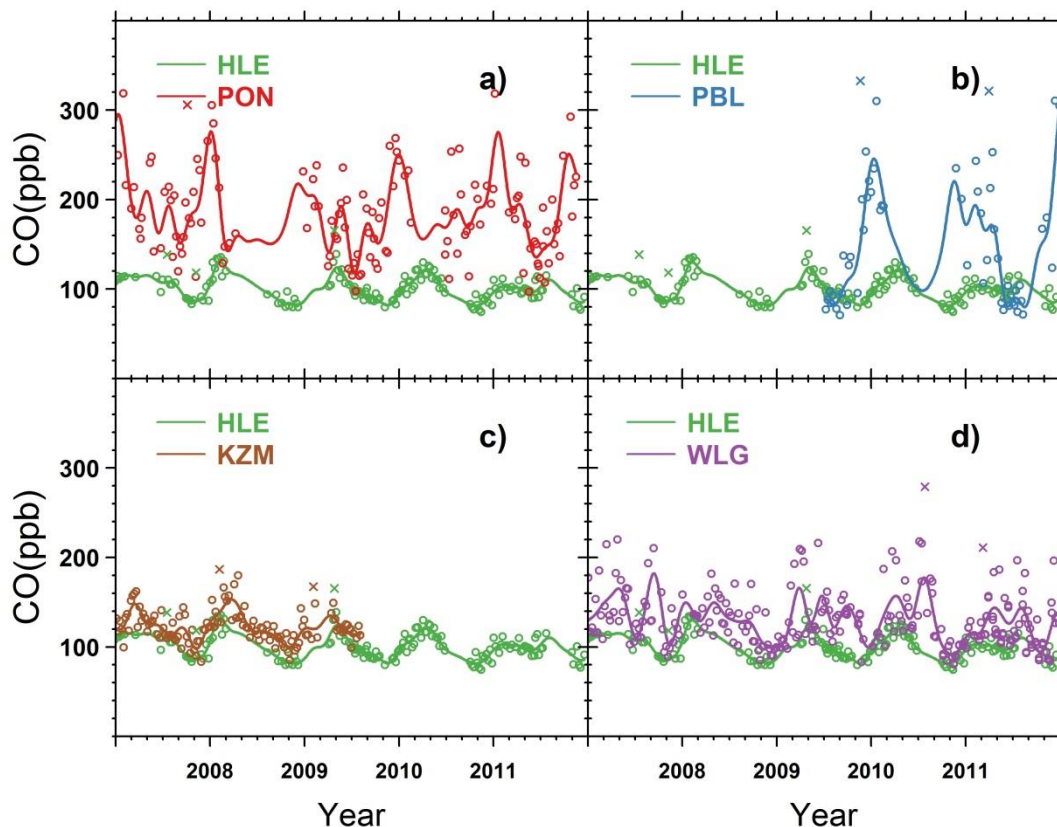1625   s.d. of 1000 bootstrap replicates.

1626
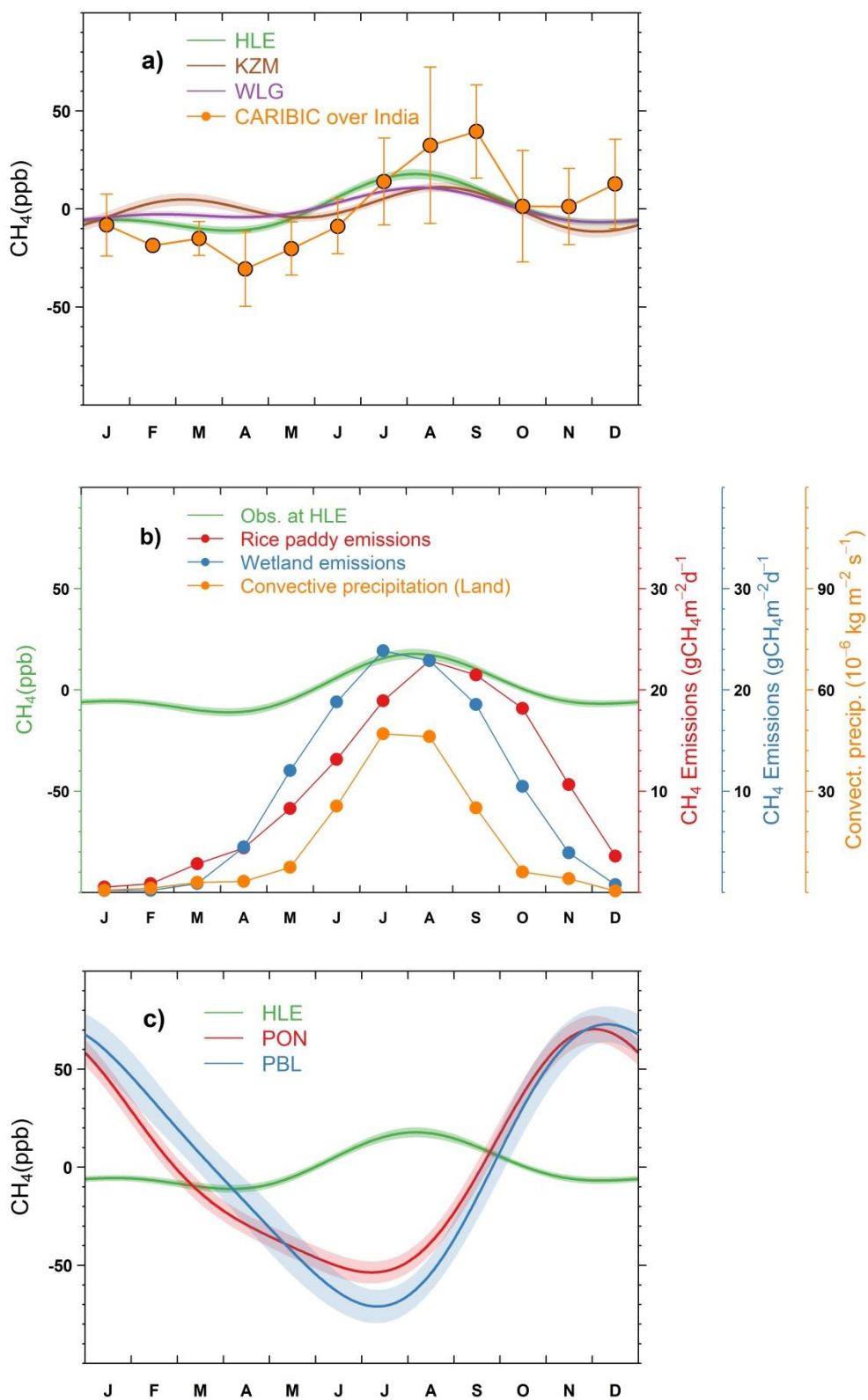
1628   **Figure 6** Time series of N$_2$O flask measurements at **(a)** HLE and PON, **(b)** HLE and PBL.

1629   The open circles denote flask data used to fit the smoothed curves, while crosses denote

1630   discarded flask data lying outside 3 times the residual standard deviations from the smoothed

1631   curve fits. For each station, the smoothed curve is fitted using Thoning's method (Thoning et

1632   al., 1989) after removing outliers.
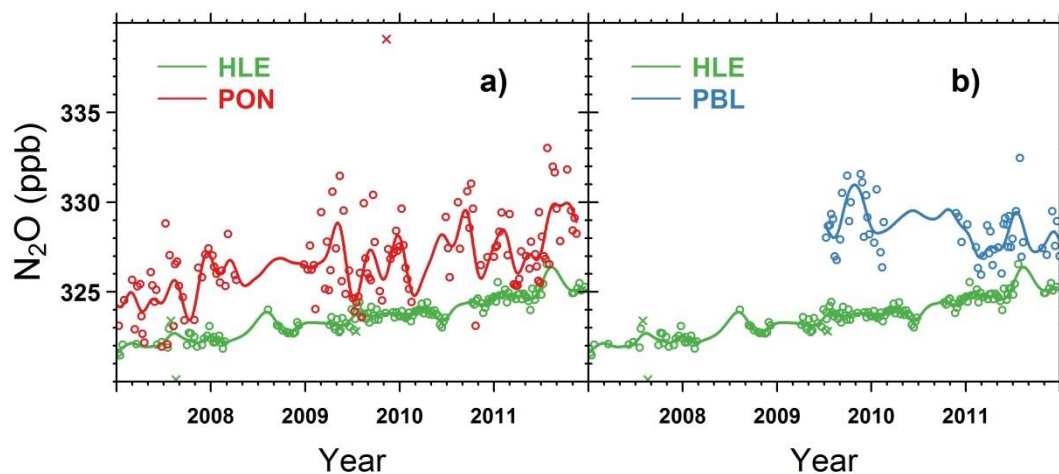
1633

1634

1635 **Figure 7** The mean N_2O seasonal cycles observed at **(a)** HLE and PON, **(b)** HLE and PBL.

1636 For each station, the mean seasonal cycle is derived from the harmonics of the smoothed

1637 fitting curve in Fig. 6. Shaded area indicates the uncertainty of the mean seasonal cycle

1638 calculated from 1 s.d. of 1000 bootstrap replicates.
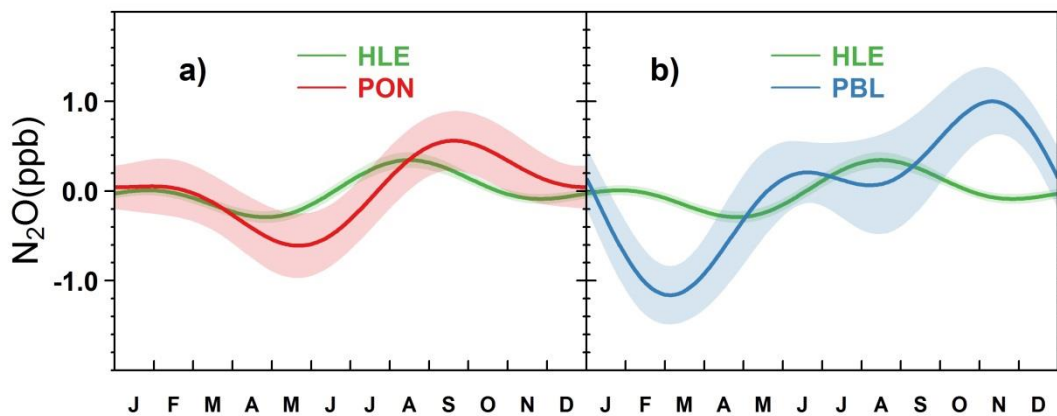
1639
1640

1641 **Figure 8** Time series of SF_6 flask measurements at **(a)** HLE and PON, **(b)** HLE and PBL, **(c)**

1642 HLE and KZM, and **(d)** HLE and WLG. The open circles denote flask data used to fit the

1643 smoothed curves. For each station, the smoothed curve is fitted using Thoning's method

1644 (Thoning et al., 1989) after removing outliers.

1645

1646

Figure 9 The mean SF$_6$ seasonal cycles observed at **(a)** HLE and PON, **(b)** HLE and PBL.

1648   For each station, the mean seasonal cycle is derived from the harmonics of the smoothed

1649   fitting curve in Fig. 8. Shaded area indicates the uncertainty of the mean seasonal cycle

1650   calculated from 1 s.d. of 1000 bootstrap replicates.

1651

1652

1653 **Figure 10** Time series of CO flask measurements at **(a)** HLE and PON, **(b)** HLE and PBL, **(c)**
1654 HLE and KZM, and **(d)** HLE and WLG. The open circles denote flask data used to fit the
1655 smoothed curves, while the crosses denote discarded flask data lying outside 3 times the
1656 residual standard deviations from the smoothed curve fits. For each station, the smoothed
1657 curve is fitted using Thoning's method (Thoning et al., 1989) after removing outliers.

1658

1659

1660   **Figure 11** The mean CO seasonal cycles observed at **(a)** HLE and PON, **(b)** HLE and PBL,

1661   **(c)** HLE and KZM, and **(d)** HLE and WLG. For each station, the mean seasonal cycle is

1662   derived from the harmonics of the smoothed fitting curve in Fig. 10. Shaded area indicates

1663   the uncertainty of the mean seasonal cycle calculated from 1 s.d. of 1000 bootstrap replicates.
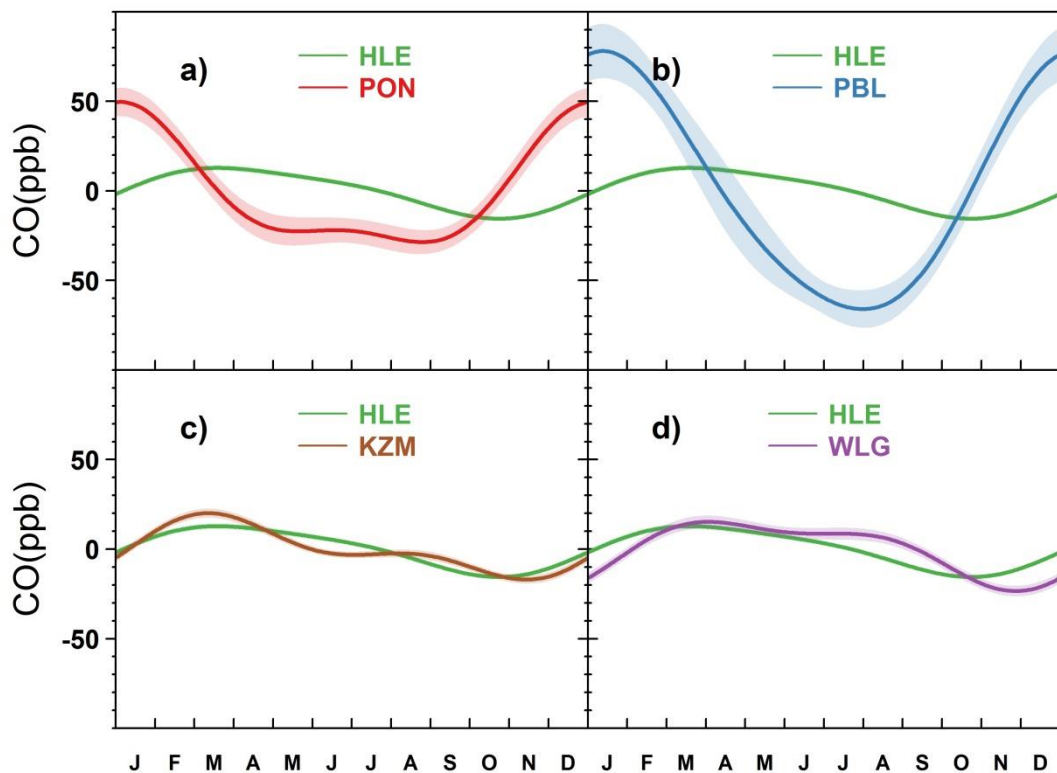

1664

1665

1666   **Figure 12** Time series of H$_2$ flask measurements at **(a)** HLE and PON, **(b)** HLE and PBL, **(c)**

1667   HLE and KZM, and **(d)** HLE and WLG. The open circles denote flask data used to fit the

1668   smoothed curves, while the crosses denote discarded flask data lying outside 3 times the

1669   residual standard deviations from the smoothed curve fits. For each station, the smoothed

1670   curve is fitted using Thoning's method (Thoning et al., 1989) after removing outliers.
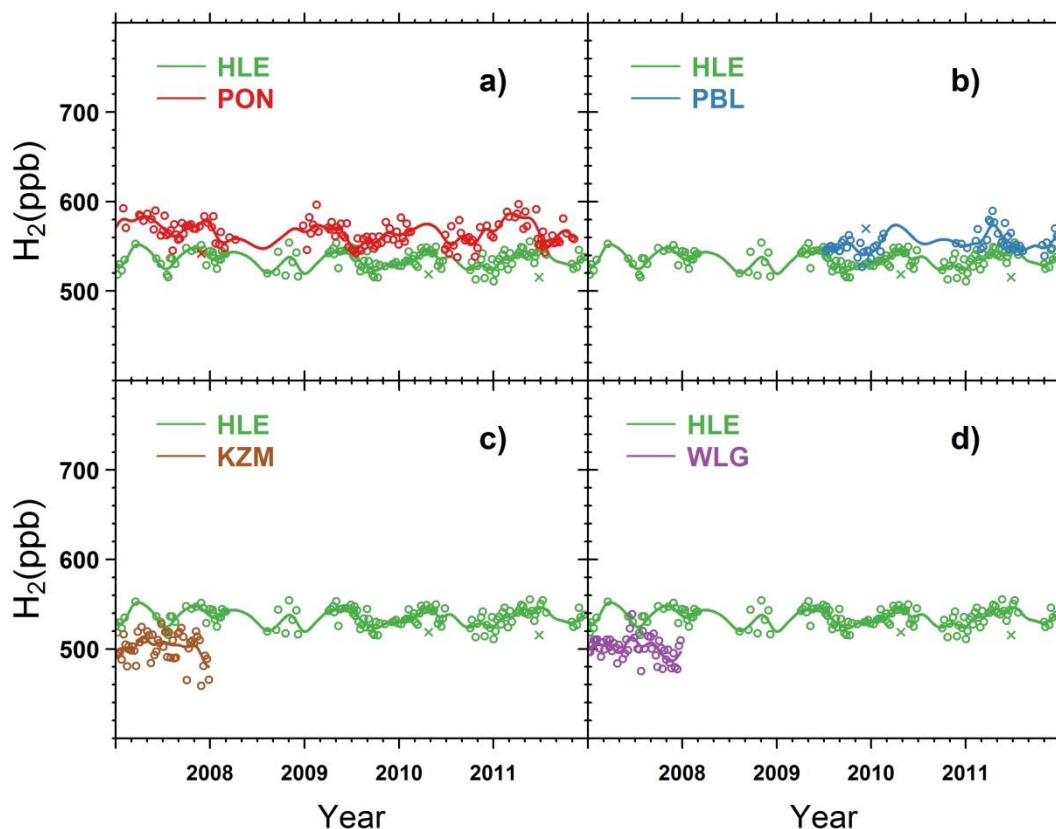
1671

1672

1673   **Figure 13** The mean H_2 seasonal cycles observed at **(a)** HLE and PON, **(b)** HLE and PBL, **(c)**

1674   HLE and KZM, and **(d)** HLE and WLG. For each station, the mean seasonal cycle is derived

1675   from the harmonics of the smoothed fitting curve in Fig. 12. Shaded area indicates the

1676   uncertainty of the mean seasonal cycle calculated from 1 s.d. of 1000 bootstrap replicates.
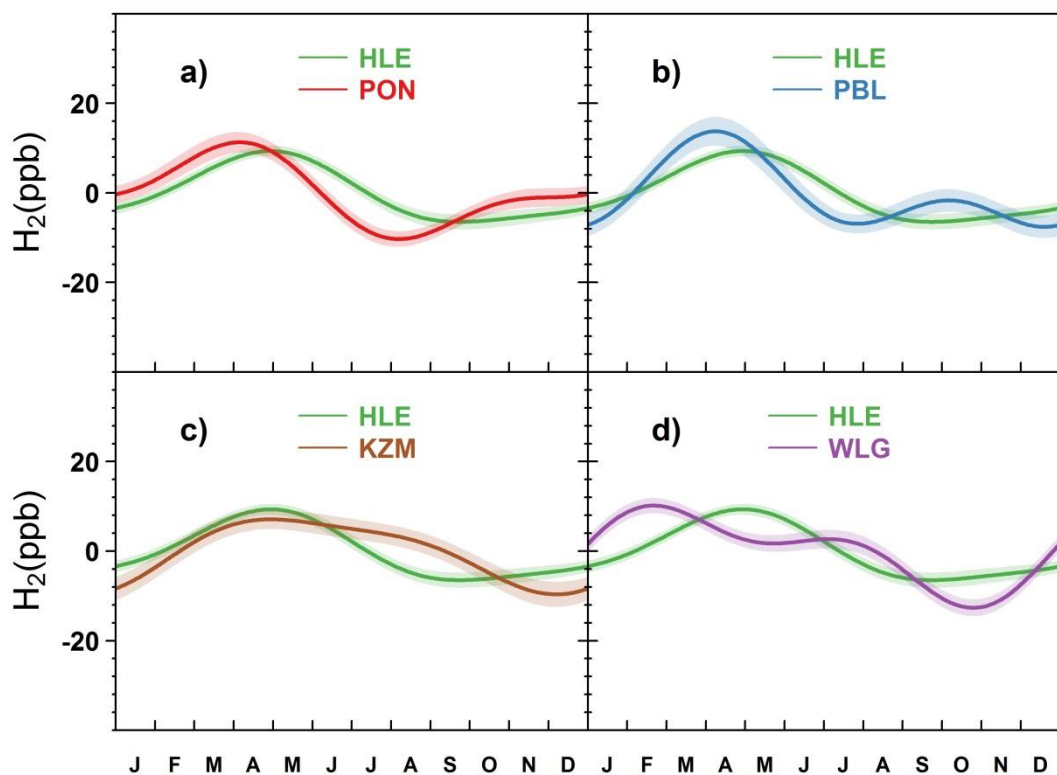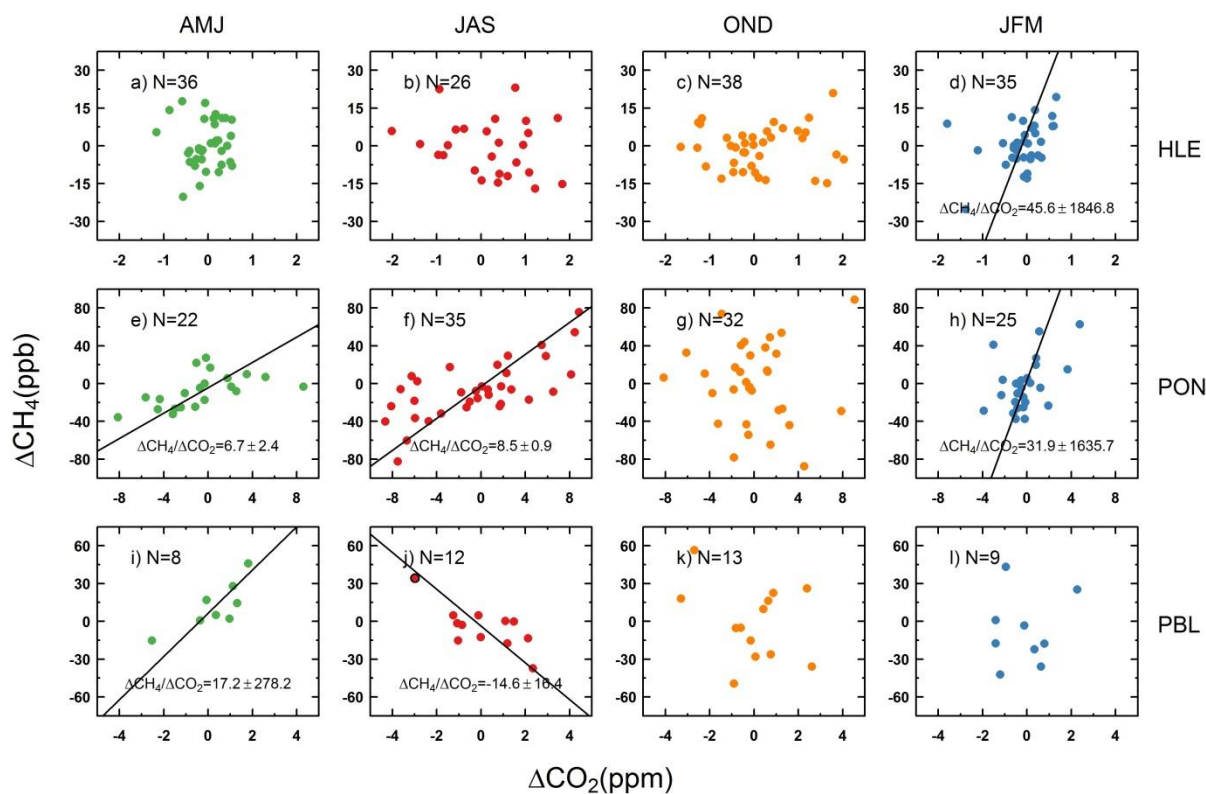

1677

1678 **Figure 14** The relationships between ΔCH₄ and ΔCO at HLE **(a–d)**, PON **(e–h)**, and PBL **(i–**

1679 **l)** for April–June (AMJ), July–September (JAS), October–December (OND), and January–

1680 March (JFM). For each panel, ΔCH₄ and ΔCO are estimated as residuals from smoothed

1681 curves. The ΔCH₄/ΔCO ratio is the slope of the fitting line from the orthogonal distance

1682 regression, with the SD calculated from 1000 bootstrap replications.
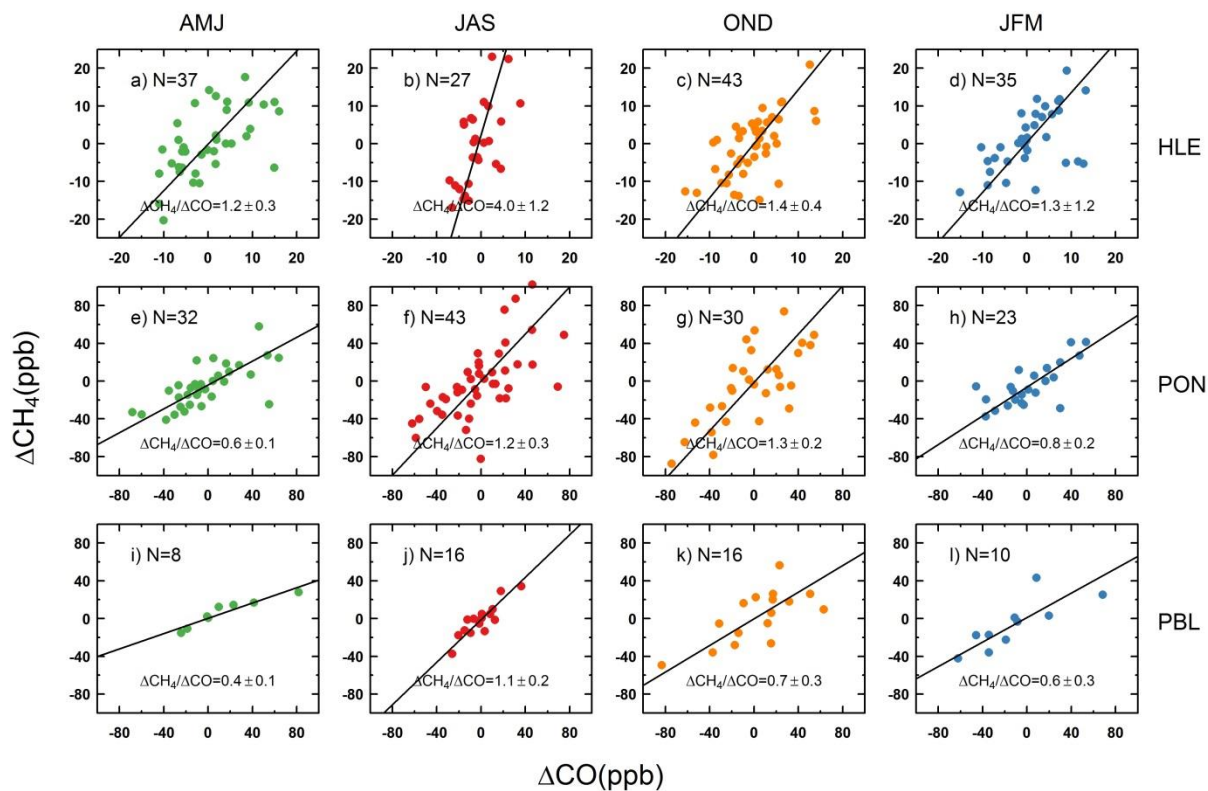

1683

1684

1685 **Figure 15** The relationships between ΔCH_4 and ΔCO_2 at HLE **(a–d)**, PON **(e–h)**, and PBL
1686 **(i–l)** for April–June (AMJ), July–September (JAS), October–December (OND), and January–
1687 March (JFM). For each panel, ΔCH_4 and ΔCO_2 are estimated as residuals from smoothed
1688 curves. The $\Delta CH_4/\Delta CO_2$ ratio is the slope of the fitting line from the orthogonal distance
1689 regression, with the SD calculated from 1000 bootstrap replications. For ΔCH_4 and ΔCO_2 that
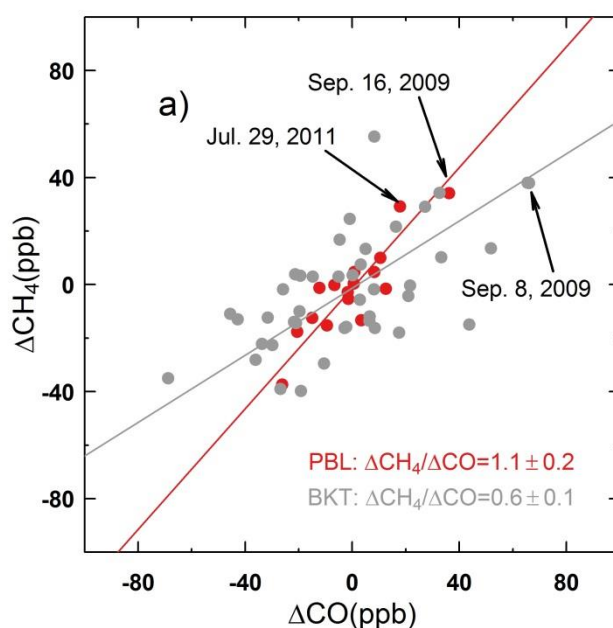1690 is not significantly correlated, the fitting line is not plotted.

1691

1692

1693   **Figure 16** The relationships between ΔCO and ΔCO_2 at HLE **(a–d)**, PON **(e–h)**, and PBL **(i–**

1694   **l)** for April–June (AMJ), July–September (JAS), October–December (OND), and January–

1695   March (JFM). For each panel, ΔCO and ΔCO_2 are estimated as residuals from smoothed

1696   curves. The $\Delta CO/\Delta CO_2$ ratio is the slope of the fitting line from the orthogonal distance

1697   regression, with the SD calculated from 1000 bootstrap replications. For ΔCO and ΔCO_2 that

1698   is not significantly correlated, the fitting line is usually not plotted.
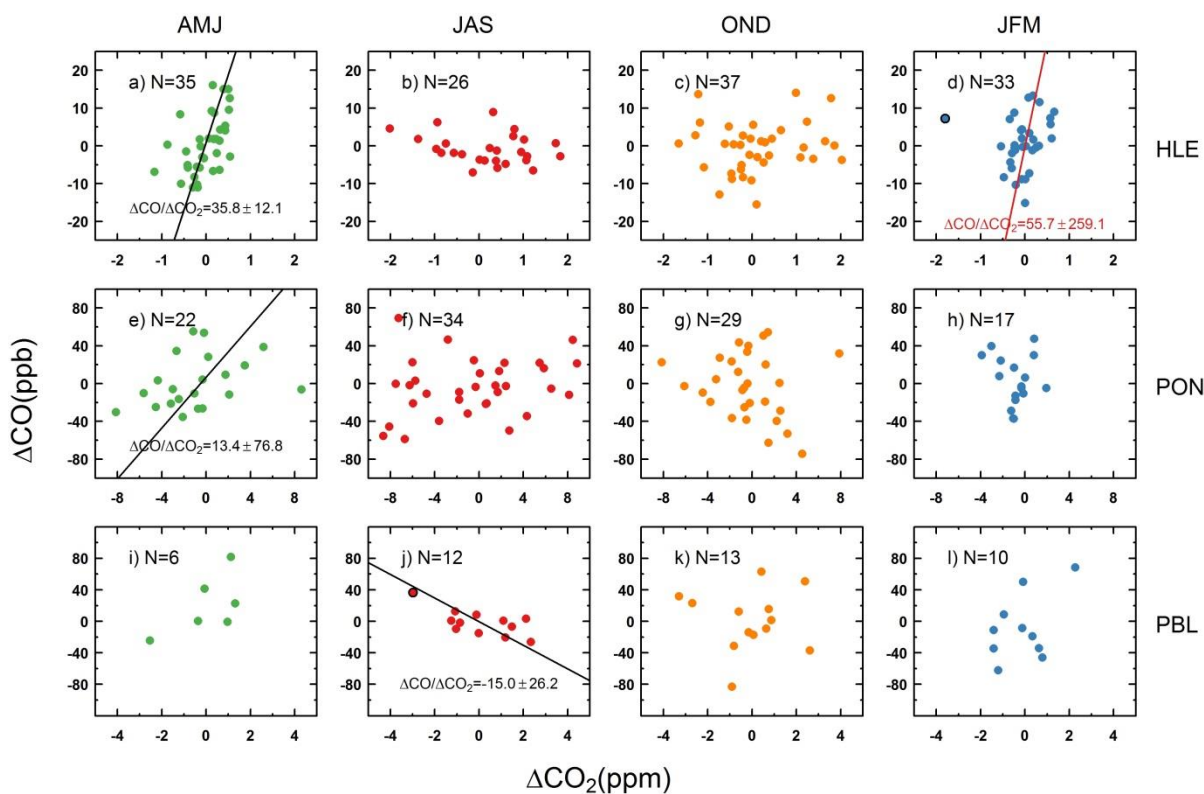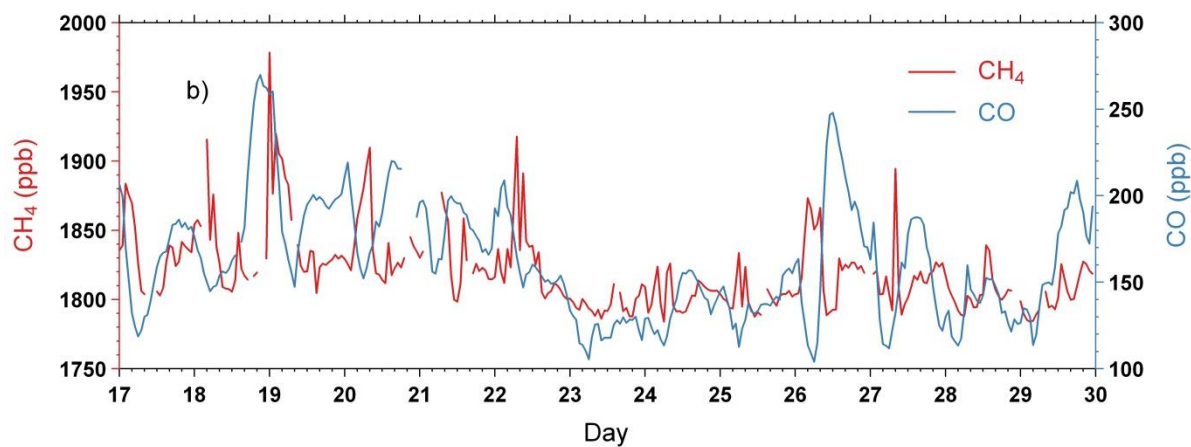

1699

1700

1701   **Figure 17 (a)** The relationship between ΔCH_4 and ΔCO at PBL (colored by red) and BKT

1702   (colored by grey) during July–September (JAS) over the period of 2007–2011. ΔCH_4 and

1703 ΔCO are estimated as residuals from smoothed curves. The $\Delta CH_4/\Delta CO$ ratio is the slope of

1704   the fitting line from orthogonal distance regression (ODR), with the SD calculated from 1000

1705   bootstrap replications. Two abnormal events at PBL are labeled, with enhancements of CH_4

1706   and CO on September 16, 2009 and July 29, 2011, respectively. Enhancements of CH_4 and

1707   CO are also observed at BKT on Sep. 8, 2009. **(b)** Hourly CH_4 and CO measurements at BKT

1708   in July, 2011 (BMKG & EMPA). Enhancements of CH_4 and CO are observed during July 17-

1709   21, 2011.

1710

1711